

043
SHA
13640

STUDIES OF INTERPLANETARY MEDIUM USING
INTERPLANETARY SCINTILLATION

by

ASHOK KUMAR SHARMA

A THESIS
SUBMITTED TO THE
GUJARAT UNIVERSITY
FOR THE DEGREE OF
DOCTOR OF PHILOSOPHY

JUNE 1988

PHYSICAL RESEARCH LABORATORY

AHMEDABAD-380 009

INDIA

043



B13640

DEDICATED

TO

MY PARENTS

C E R T I F I C A T E

I hereby declare that the work presented in this thesis is original and has not formed the basis for the award of any degree or diploma by any University or Institution.



ASHOK KUMAR SHARMA

(AUTHOR)

Physical Research Laboratory

Ahmedabad 380 009, India

Certified by:


S.K. ALURKAR
(Professor-in-Charge)
Physical Research Laboratory
Ahmedabad 380 009, India

STATEMENT

The work presented in this thesis was carried out by the author during 1983-1987. This is the first thesis comprising the results obtained by using Radio telescope at Thaltej near Ahmedabad (India), operating at 103 MHz.

This thesis contains seven chapters in all.

An introduction to the thesis is given in Chapter 1. This contains, in brief, a description of Interplanetary Medium (IPM), cometary studies, etc. The other two problems regarding change in apparent position of a quasar by the large-scale irregularities and IPS observation of PSR 0531+21, discussed in the thesis, are also mentioned in this chapter.

Chapter 2 describes briefly Interplanetary Scintillation (IPS) phenomenon and its use in carrying out the studies presented in this thesis. A relevant theory of IPS is given in the same Chapter. Effects of sourcesize and receiver band-width on scintillations are also described.

Description of radio telescope used for the present investigations is given in Chapter 3. This system consists of a fullwave dipole antenna, correlation receiver, scintillometer and analog and digital data recording devices. Salient features of these devices and their calibrations are discussed in the same Chapter.

Chapter 4 presents the observations of the radio source 3C459 occulted by the ion-tail of Comet Halley. These observations were made in December 1985. Plasma density irregularities in the tail and their scale-size are calculated to be $\sim 2/\text{c.c.}$ and 100 Km respectively. Plasma density is estimated to be $\sim 200/\text{c.c.}$ in the ion-tail. Here, the main assumption has been that the ratio of ambient solar plasma density and its irregularity is same as that of in the case of the cometary plasma at any heliocentric distance. These observations have contributed significantly to the cometary studies. Similar other studies reported elsewhere are also discussed.

During the observations of a quasar 3C 298 an apparent sinusoidal variation on recording was noted. It was believed to be due to refraction effect caused by large-scale plasma density irregularities across the line of sight. An attempt is made to understand the origin of the same. From the present study, change in apparent position of the quasar is estimated to be ~ 5 arcmin. This is described in Chapter 5.

The last important problem, which is presented in Chapter 6, is about the use of IPS technique for the study of the compact source PSR 0531+21 in the Crab Nebula. Using this technique its angular size and scintillating flux are estimated to be ~ 0.16 arcsec and ~ 100 Jy respectively.

In the last Chapter studies for future, using IPS technique, are outlined as follows:

- (i) Co-ordinated observations should be made regarding occultation of a radio source by an ion-tail of a comet and of scintillating radio sources
- (ii) A catalogue at 103 MHz should be made. This will be useful for interplanetary weather studies, etc.

ACKNOWLEDGEMENTS

I express my gratitude to my Ph.D. Thesis Supervisor Prof. S.K. Alurkar for his guidance and help throughout my doctoral work. I thank him for critically going through the manuscript and making several useful suggestions. Thanks are due to Prof. R.V. Bhonsle for encouragement and useful advice. I sincerely thank my senior colleague and friend Dr. H.O. Vats who helped me in all possible ways.

I am thankful to Messrs S.L. Kayastha, A.H. Desai, A.D. Bobra, S.K. Shah, K.J. Shah, N.S. Nirman, R. Sharma, P. Venat and Janardhan P. for various types of help provided during the course of this work.

Thanks are also due to Prof. S.S. Degaonkar for useful discussions I had with him.

The contribution of all the members of Radio Astronomy Group of PRL is also acknowledged, without their support this work would not have been possible.

Thanks are due to Messrs A. Narayan, Maqbool Ahmed, G. Beig, K.P. Subramanian, Debi Prasad, and Drs. Shyam Lal and T. Chandrasekhar, who helped me in some or the other way in carrying out the studies.

I thank all my friends and well wishers in and outside the PRL who helped me in various ways and whose company I enjoyed a lot.

I acknowledge the help rendered by different facilities of PRL.

I sincerely thank Profs. S.P. Khare, B.B. Srivastava and T.P. Sharma, Physics Department, Institute of Advanced Studies, Meerut University, Meerut, who advised and encouraged me to join PRL for my Ph.D. studies.

I am thankful to Messrs K.T. John, D. Stephen and Mrs. M.V. Vijayalakshmi for neatly typing the manuscript.

I take this opportunity to express my gratitude to my parents-in-law for their blessings, love and unwavering support during the course of the present work. The cheerful attitude and affection of my brothers, sisters, brothers-in-law and sister-in-law has been a great help during the present studies.

My appreciation is due to my wife, ANJU, for profound understanding, moral support, co-operation and great patience during the course of this work. This cannot be expressed in words. I am most grateful to her.

Ashok Kumar Sharma

PRL, Ahmedabad

June 1988

LIST OF PUBLICATIONS

1. 103 MHz Interplanetary Scintillation Observation of PSR0531+21
(S.K. Alurkar, H.O. Vats, R.V. Bhonsle and A.K. Sharma)
Presented at Recent Advances in the Understanding of Structure and Dynamics of the Heliosphere; Joint US-Japan Seminar, Kyoto, Japan, 1984.
2. Detection of Large Scale Electron Density Irregularities During IPS Observations at 103 MHz
(S.K. Alurkar, H.O. Vats, R.V. Bhonsle and A.K. Sharma)
Proc. Indian Acad. Sci. (Earth Planet. Sci.) 94, 77, 1985.
3. * Exploration of Heliosphere by Interplanetary Scintillation
(R.V. Bhonsle, S.K. Alurkar, S.S. Degaonkar, H.O. Vats and A.K. Sharma)
Proceedings of the 19th ESLAB Symposium on the Sun and the Heliosphere in Three Dimensions, Les Diablerets, Switzerland, June 4-6, 1985. Edited by R.G. Marsden, p.153, 1986.
4. * The Great Solar Flare of 24 April, 1985 and Associated Interplanetary and Ionospheric Effects Observed at Ahmedabad
(R.V. Bhonsle, S.K. Alurkar, H.O. Vats, A.K. Sharma, Harish Chandra and G.D. Vyas)
Presented at the STIP Symposium on Retrospective Analysis and Future Coordinated Intervals, Les Diablerets, Switzerland, 10-12 June 1985,
5. Radio Observations of PKS 2314+03 During Occultation by Comet Halley
(S.K. Alurkar, R.V. Bhonsle and A.K. Sharma)
Nature, 322, 439, 1986.
6. Interplanetary Scintillation of PKS 2314+03 During Occultation by Comet Halley
(S.K. Alurkar, R.V. Bhonsle and A.K. Sharma)
(Adv. Space Res. 5, 297, 1986.
7. Occultation of Compact Radio Sources by the Ion-Tail of Halley's Comet
(S.K. Alurkar, A.K. Sharma and R.V. Bhonsle)
Presented at the STIP Symposium on Physical Interpretation of Solar/Interplanetary and Cometary Intervals, Huntsville, Alabama, USA, 12-15 May, 1987.

* The work presented in this paper is not included in the thesis.

8. Enhanced Scintillations Caused by Cometary Plasma
Tails
(S.K. Alurkar, A.K. Sharma, P. Janardhan and R.V.
Bhonsle)
(Communicated)

CONTENTS

CERTIFICATE

STATEMENT

ACKNOWLEDGEMENT

LIST OF PUBLICATIONS

CHAPTER ONE : INTRODUCTION	1.1
CHAPTER TWO : INTERPLANETARY SCINTILLATION AND RELEVANT THEORY	2.1
2.1 Interplanetary scintillation	2.1
2.2 Relevant theory	2.2
CHAPTER THREE : THE RADIO (IPS) TELESCOPE AT THALTEJ	3.1
3.1 Introduction	3.1
3.2 Basic considerations for the design of the IPS telescope	3.3
3.3 The radio (IPS) telescope at Thaltej	3.7
3.4 Calibration	3.22
3.5 Specifications of the radio telescope at Thaltej	3.27
CHAPTER FOUR : ENHANCED SCINTILLATION OF A RADIO SOURCE CAUSED BY THE ION-TAIL OF THE COMET HALLEY	4.1
4.1 Introduction	4.1
4.2 Observations	4.1
4.3 Data analysis and results	4.5

4.4	Discussion	4.7
4.5	Conclusions	4.15
	APPENDIX I	4.27

CHAPTER FIVE : DISPLACEMENT OF INTENSITY PATTERN PRODUCED BY LARGE- SCALE DENSITY IRREGULARITIES	5.1
--	-----

5.1	Introduction	5.1
5.2	Observations	5.4
5.3	Analysis and results	5.7
5.4	Discussion and conclusion	5.9

CHAPTER SIX : IPS OBSERVATIONS OF PSR 0531+21	6.1
--	-----

6.1	Introduction	6.1
6.2	Observations	6.3
6.3	Analysis and results	6.3
6.4	Discussion and conclusion	6.7

CHAPTER SEVEN : FUTURE WORK	7.1
-----------------------------	-----

REFERENCES

CHAPTER ONE

INTRODUCTION

It is believed that the Sun-Earth system is situated in a huge bubble, called heliosphere. This heliosphere is formed due to the interaction of solar wind and interstellar medium. The solar wind is the supersonic flow of high temperature plasma from the solar corona. This becomes supersonic beyond a distance of about 6 solar radii (Dryer, 1987) and attains a velocity of about 300-400 Km/s when the Sun is quiet and ~ 600 Km/s when it is disturbed. The extent of this solar wind flow is at least upto the orbit of Uranus. Cosmic processes occurring in this vast heliosphere are to a large extent controlled and shaped by this supersonic wind. Hence, the study of the physics of the heliosphere is fundamental to the understanding of various solar-terrestrial phenomena.

Till the first half of this century, interplanetary space was believed to be a dusty vacuum. Biermann (1951) suggested that the acceleration and ionization of cometary molecules were due to the interaction with an interplanetary background of ions flowing continuously and radially from the Sun. The expected flux of these ions was about $10^{10}/\text{cm}^2/\text{s}$ near the Earth. The second observational evidence of the outflowing plasma was the zodiacal light, traditionally attributed to the scattering of sunlight by interplanetary dust particles. It was found to be polarized. Behr and Siedentopf (1953) argued strongly that such an effect cannot be produced by scattering from dust but from electrons with a density of about $10^3/\text{c.c.}$ near the Earth. Combination of this density with the flux value inferred by Biermann led to an estimated ion speed of about 10^2 Km/sec.

None of these hypotheses is accepted today. Flux of ions, directly observed, are two orders of magnitude lower than those inferred from the original model (Biermann, 1951). Spacecraft observations made in interplanetary space yield electron densities two orders of magnitude lower than those inferred from the theories of electron scattering.

Parker (1958, 1963) considered a new theoretical possibility, a corona expanding steadily rather than static Chapman (1957).

Parker also considered the implication of a continuous coronal expansion with regard to the nature and configuration of the interplanetary magnetic field. Hot coronal plasma would be expected to have an extremely high electrical (as well as thermal) conductivity. In such a fluid, the concept of "frozen-in" magnetic field lines (i.e. very slow diffusion of plasma transverse to the magnetic field), is applicable. The continuous flow of coronal material into interplanetary space then must result in a transport of the solar magnetic field into the interplanetary region. Thus, as the solar wind flows out from the Sun, it drags solar magnetic field lines with it. The Sun rotates with a (latitude dependent) period of 25 days for a stationary interplanetary observer (or 27 days for an observer with the orbital motion of the Earth). As a direct consequence of solar rotation, the magnetic field is drawn out to form Archimedean spirals on cones of constant heliographic latitude.

When normally smooth flow of the solar wind is made unusually turbulent (for example, by a passing shock front from the solar flare ejecta), the frozen-in field lines are tangled, and such relatively localized clumps of kinky field lines can scatter electromagnetic waves in random directions.

Parker considered some possible mechanisms for the production of disordered fields through plasma insta-

bilities that are caused by pressure anisotropies. One such instability is the fire-hose instability, which occurs when the pressure perpendicular to the magnetic field (P_{\perp}) is less than the pressure parallel to the field (P_{\parallel}) according to the relation (Brandt, 1970)

$$P_{\parallel} - P_{\perp} > B^2/4\pi \quad \dots(1.a)$$

this is the condition of instability.

The other instability is the mirror instability which could be important in the solar wind beyond the Earth.

The instability criterion is (Brandt, 1970)

$$\frac{P_{\perp}}{P_{\parallel}} > P_{\perp} + \frac{B^2}{8\pi} \quad \dots(1.b)$$

Growth rates for the mirror instability are usually comparable with those of the fire-hose instability.

However, fluctuations in the solar wind magnetic field near the Earth could be interpreted as magneto-acoustic waves, which could originate at the Sun or from the interaction of fast and slow plasma streams. The tangential velocity discontinuities are, in fact, the boundary between the two fluids in relative motion parallel to the boundary and, hence subject to the Kelvin-Helmholtz insta-

bility. This instability could be the mechanism for wave production from the many discontinuities found observationally.

Irregularities present in the IPM scatter electromagnetic radiation from galactic and extragalactic sources.

To study the IPM, various techniques have been adopted. Its in-situ study has been made by spacecraft within $\pm 10^\circ$ of the ecliptic plane. Beyond this, and very close to the Sun, these are incapable of making observations. There is only one technique, called interplanetary scintillation (IPS), which can investigate the IPM away from the ecliptic. This technique, described in Chapter 2, is relatively inexpensive.

Comets visit our inner solar system periodically. Strong comets, when they approach the Sun within 2-3 AU, develop distinctive tails plasma and dust tails. This is due to the solar thermal and ultraviolet radiation which cause the material in the cometary nucleus to sublimate and ionize. Comets away from the Sun have only a nucleus of a few kilometers in size covered by ices of CO_2 , H_2O , etc. mixed with dust.

Due to the pressure of the solar wind, interplanetary magnetic field lines are curved around the cometary coma in the anti-Sunward direction. Cometary ionized material follow these field lines and the plasma tail of a

comet is formed (Alfven, 1957). The existence of solar wind was ascertained from the cometary ion-tail orientation (Brandt, 1970).

Studies of comets have been made by using different techniques such as groundbased optical and radio telescopes and in-situ measurements using space platforms. In the present thesis mainly ground-based radio astronomical observations of comets will be presented.

The plasma density in the region of the cometary coma and tail has been estimated from optical data by Wurm (1968) to be about 10^3 ions/c.c. Conway et al. (1961) gave an upper limit from radio data of 10^6 ions/c.c. If density irregularities are present in the plasma tail of a comet, radio waves from a compact source passing through them will be scattered, resulting in fluctuations in its intensity as in the IPS phenomenon described in Chapter 2. Whitfield and Hogbom (1957) attempted to observe the angular broadening of radio sources as they got occulted by comet Arend-Roland (1956 h). No broadening above the angular resolution limit of their interferometer, which was about 30 arcmin. at 3.7 m wavelength, was detected. This provided an upper limit of 10^4 el/c.c. for the r.m.s. fluctuations in the electron density in the comet.

Ananthakrishnan et al. (1975) observed strong fluctuations in the intensity of the radio source PKS 2025-15 at 327 MHz during its occultation by comet Kohoutek on

5 January, 1974. They reported that no unique explanation could be given of the intensity fluctuations with 10 sec. periodicity in terms of scintillations produced by the cometary plasma tail. Lee (1976) has, theoretically shown that the observations of Ananthakrishnan et al. (1975) could be interpreted as scintillations caused by the turbulent plasma in the comet's tail.

As the above study remained inconclusive, observations of occultation of a quasar 3C 459 by the ion-tail of comet Halley were made in December 1985. These are described in chapter 4 of this thesis. Following our work other observations were also reported by Slee et al. (1987), Ananthakrishnan et al. (1987) and Hajivassiliou and Duffett-Smith (1987). These are discussed and compared with our observations in the same chapter.

In this thesis, apart from the radio astronomical study of the Halley's comet, two other problems have also been presented. These are displacement of intensity pattern produced by large-scale density irregularities and IPS observations of PSR 0531+21.

During observations of a quasar, an apparent sinusoidal variation of the analogue recording of its scintillating pattern was observed. This pattern was believed to be due to refraction effect caused by large-scale plasma density irregularities lying across the line of sight.

An attempt is made in Chapter 5 to understand the origin of such irregularities. The last important problem presented in Chapter 6 is about the use of IPS technique for the study of the compact source PSR 0531+21 in the Crab Nebula. Using this technique its angular size and scintillating flux are estimated.

CHAPTER TWO

INTERPLANETARY SCINTILLATION AND RELEVANT THEORY

2.1 Interplanetary Scintillation

The phenomenon of interplanetary scintillation (IPS) is a radio analog of the twinkling of stars in the night sky and atmospheric scintillation of laser beams. As shown in Figs. 2.1 and 2.2, when radio waves from a distant compact source enter the interplanetary medium (IPM) containing solar plasma they are scattered by the plasma density irregularities. If the radio source is sufficiently small in diameter so that the plasma density irregularities are illuminated coherently, phase modulations are imposed on the plane wavefront. Emerging out from the main bulk of

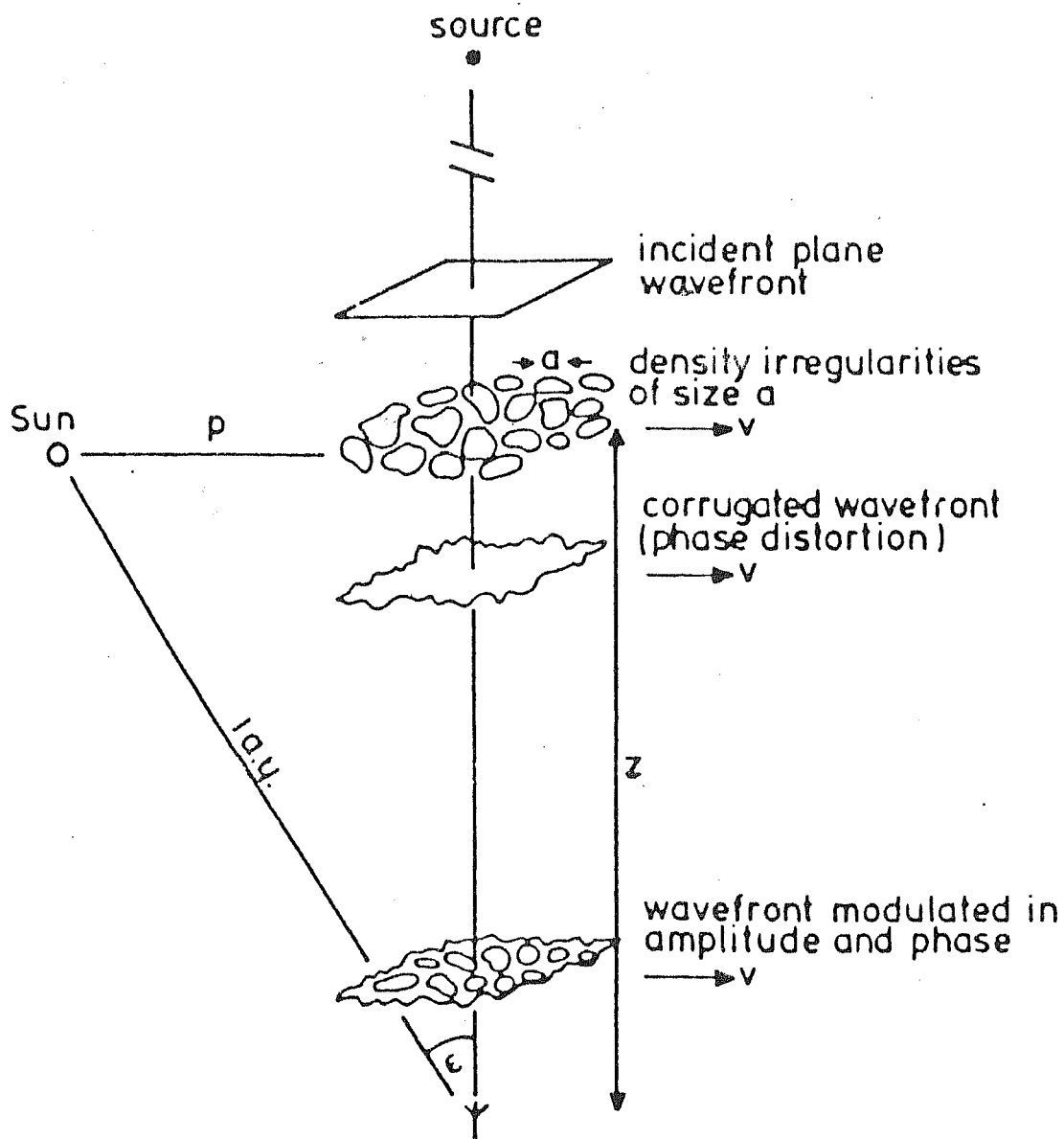


Fig.2.1 IPS geometry

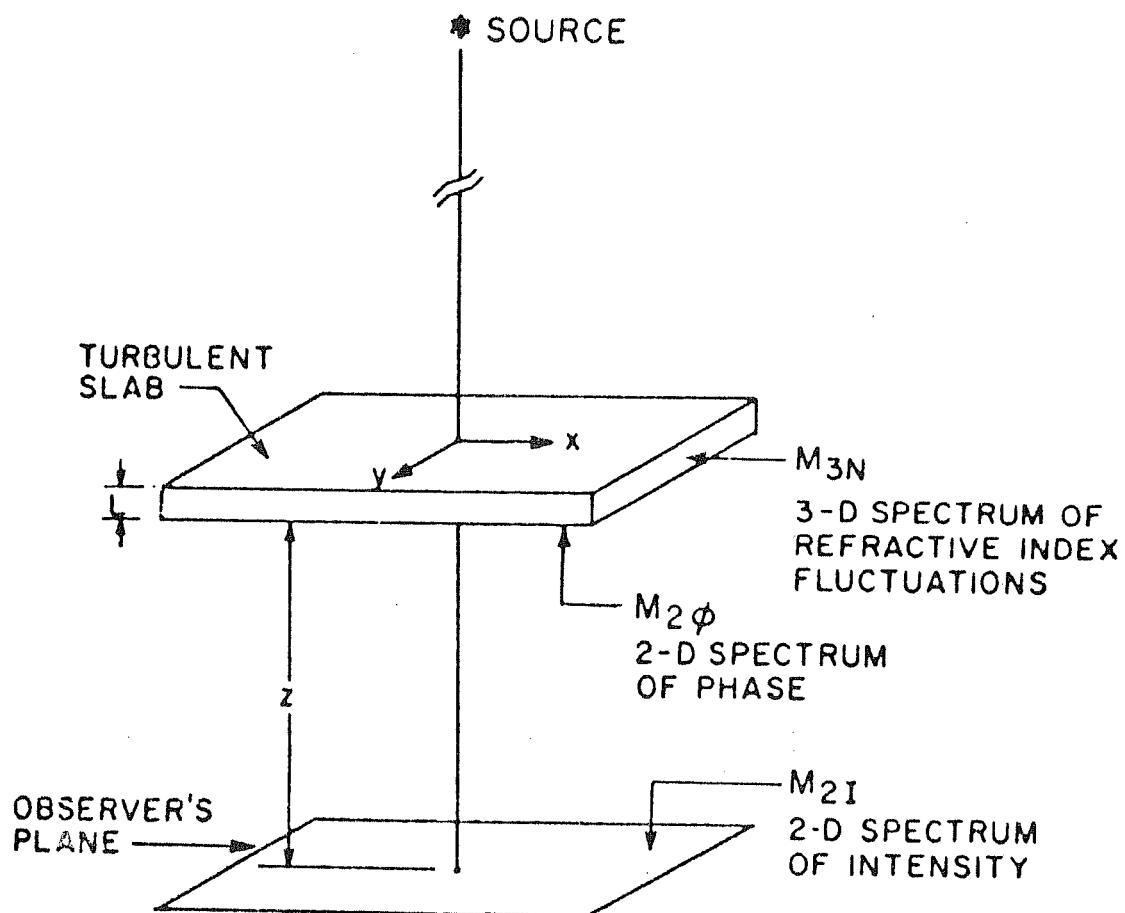
the scattering medium, these phase-modulated waves propagate in the IPM and interfere with one another, consequently causing at the Earth variations of intensity of the radio source. As a result of the solar wind flow across the line of sight to the source, the spatial distribution of the plasma density variation in the scattering medium is converted into temporal fluctuations of intensity at the observing site, with a typical fluctuation period of one second.

Thus, the IPS method provides essentially a 1-dimensional scan of the scattering region. Radio sources with angular sizes of about 1.0 arcsec. or less cause IPS yielding a temporal spectrum ranging from, say 0.1 to about 3 Hz. The scintillators are mainly extragalactic radio sources, such as radio galaxies and quasars, a fraction or whole of which is effective as scintillating radio sources.

Since the discovery of IPS (Hewish et al. 1964), many systematic studies have been made. The method of IPS and the results obtained have been reviewed extensively by Cohen (1969), Hewish (1972), Jokipii (1973), Coles et al. (1974), Lotova (1975) and Little (1976). The IPS observations have been used for

- (a) investigating the IPM (Houminer, 1971; Armstrong, 1975; Coles and Rickett, 1976; Dennison and Wiseman, 1968)

INTENSITY SPECTRA ON OBSERVER'S PLANE DUE TO TURBULENT SLAB



$$M_{2\phi}(q_x, q_y) = \frac{4\pi^2}{\lambda^2} \cdot L \cdot M_{3N}(q_x, q_y, q_z = 0)$$

$$M_{2I}(q_x, q_y) \approx 4 \sin^2\left(\frac{q^2 \lambda z}{4\pi}\right) M_{2\phi}(q_x, q_y)$$

Fig. 2.2 Schematic of spectra at various planes during IPS observations.

- (b) determining the structure of compact galactic and extragalactic radio sources (Cohen et al. 1967; Little and Hewish, 1966; Armstrong et al. 1973; Duffett-Smith, 1976), and
- (c) estimation of solar wind velocity (Hewish and Symonds, 1969; Lovelace et al. 1970; Coles and Maagoe, 1972; Armstrong and Coles, 1972; Watanabe et al. 1973).

Recently, attempts have also been made to study ion-tails of comets using the IPS technique.

In the present thesis some of the above mentioned studies have been presented. All the work presented in this thesis is based on the interpretation of weak scattering intensity scintillation data. Here a brief review of fundamentals of scintillation theory is given. Weak scattering theory has been well understood for quite sometime and here it will not be repeated. The reader is referred to Ratcliffe (1956), Tatarski (1961), Salpeter (1967), Readhead (1971 and Ishimaru (1972) for further details of the theory.

The measurables in scintillation are statistical moments of the incident electric field like scintillation index, intensity spectrum, etc. Theory relates these to statistics of the random medium.

2.2 Relevant Theory

A plane wave propagating from a distant compact

radio source is incident on a thin phase changing slab of the plasma turbulence. Immediately outside the slab the wavefront gets corrugated due to phase deviations. After propagating a certain distance, called Fresnel distance $Z_F \approx 2\pi a^2/\lambda$ (where 'a' is the scale-size of irregularities and λ is the operating wavelength) through free space to the observer, amplitude modulations start building up, forming a spectrum of intensity on the ground (Fig. 2.2).

The statistical quantity of the medium that is of interest, here is the 3-dimensional spatial spectrum of refractive index fluctuations at operating radio wavelength $\lambda, M_{3ne}(\underline{q})$. In a plasma, it can be related to the 3-dimensional electron density spectrum by

$$M_{3N}(\underline{q}) = r_e^2 \lambda^2 M_{3ne}(\underline{q}) \quad \dots(2.a)$$

where $\underline{q} = (q_x^2 + q_y^2 + q_z^2)^{1/2}$, is 3-dimensional wavenumber and r_e is the classical electron radius.

If the slab thickness $L \gg a$, ^{the} correlation scale of the medium (scale-size of the irregularity), ^{then} outside the slab 2-dimensional spatial phase spectrum for thin screen ($L \ll Z$, Salpeter, 1967) is expressed as

$$M_{2\phi}(q_x, q_y) = \frac{4\pi^2}{\lambda^2} L \cdot M_{3N}(q_x, q_y, q_z=0) \quad \dots(2.b)$$

(neglecting the variation in Z direction)

Free space propagation of the phase distorted waves results in intensity scintillation (spectrum of intensity) on the observer's plane. Under weak scattering conditions (r.m.s. phase deviation, $\phi_0 \ll 1$ radian), 2-dimensional intensity spectrum can be written as

$$M_{2I}(q_x, q_y) = 4 \sin^2 \left(\frac{q^2 \lambda z}{4\pi} \right) \cdot M_{2\phi}(q_x, q_y) \quad \dots(2.c)$$

where the term $4 \sin^2 \left(\frac{q^2 \lambda z}{4\pi} \right)$ is a high-pass "propagation filter" which removes the lower spatial frequencies from the spectrum.

Scintillation index, m is defined as (Readhead et.al. 1978)

$$m^2 = \iint M_{2I}(q_x, q_y) dq_x dq_y \quad \dots(2.d)$$

In the direction of propagation along the x-axis (Fig. 2.2), 1-dimensional intensity temporal spectrum becomes

$$M_I(f) = \frac{4\pi}{V_x} \int_{-\infty}^{\infty} M_{2I}\left(q_x = \frac{2\pi f}{V_x}, q_y\right) dq_y, \text{ for } f \geq 0 \quad \dots(2.e)$$

where V_x is the X-component of the velocity of the plasma density irregularities.

Actually, the pattern received by the observer is made up of contributions from scattering volume all along the line of sight. In the case of weak scattering, the spectrum can be approximated as (Sime, 1976)

$$M_I'(f) = \int_0^Z M(f, z) dz \quad \dots(2.f)$$

Some of these equations in modified form have been used in subsequent chapters.

2.2(a) Effect of source size

Finite source size reduces the scintillations. This effect can be used for deducing angular size of scintillating sources. If $M_{2I_{\text{ext}}}(\underline{q})$ and $M_{2I_{\text{pt}}}(\underline{q})$ are 2-dimensional intensity spectra for an extended and a point source respectively, then

$$M_{2I_{\text{ext}}}(\underline{q}) = M_{2I_{\text{pt}}}(\underline{q}) |V(\underline{q}, z)|^2 \quad \dots(2.g)$$

(commonly known as Cohen-Salpeter equation, Salpeter, 1967),

where $V(\underline{q}, z)$ is called the source visibility defined as

$$|V(q, z)|^2 = \frac{m_{\text{ext}}}{m_{\text{pt}}} \leq 1$$

where m_{ext} and m_{pt} are scintillation indices for extended and point sources respectively. Thus, m_{ext} acts as a low-pass filter, reducing higher spatial frequencies from the irregularity spectrum.

2.2(b) Effect of finite receiver band-width

Finite receiver band-width also reduces scintillations,

$$M_{2I}(\underline{q}) = M_{2I}(\underline{q}) \rho^2(\tau) \quad \dots(2.h)$$

as given by Cronyn (1970). The term $\rho^2(\tau)$ is called the bandwidth filter.

The effect of both finite source diameter and band-width is to cause a reduction of the scintillations as they both act as low pass filters on the spatial spectrum. To judge the relative importance of these two filters one can compare the effects of an isotropic gaussian source to a rectangular bandpass. By equating the e^{-1} widths of these two filters one may express the bandwidth effect in terms of an effective source diameter. (Full width at e^{-1}). This equivalent diameter is given as $\phi_e = \frac{1}{\pi} \left(\frac{2\Delta f \cdot \lambda}{f \cdot Z} \right)^{\frac{1}{2}}$ where ϕ_e is the equivalent diameter in radians, λ is the

centre wavelength, Z is the distance to the screen and $\frac{\Delta f}{f}$ is the fractional bandwidth (full width) of the rectangular band pass (Scott, 1970).

All the equations described earlier are valid for gaussian and power-law models of the IPM.

CHAPTER THREE

THE RADIO (IPS) TELESCOPE AT THALTEJ

3.1 Introduction

A triangular network of three Radio (IPS) Telescopes (R.Ts) operating at a frequency of 103 MHz has been commissioned since early 1987 by the Radio Astronomy group of the Physical Research Laboratory, Ahmedabad, India. The main scientific objectives of this R.T. system are, among others, the following:

- (i) To study short and long-term characteristics of the plasma turbulence in the interplanetary medium (IPM) in the range of about 0.3-1 AU from the Sun, and

GEOMETRY OF THE THREE IPS STATIONS

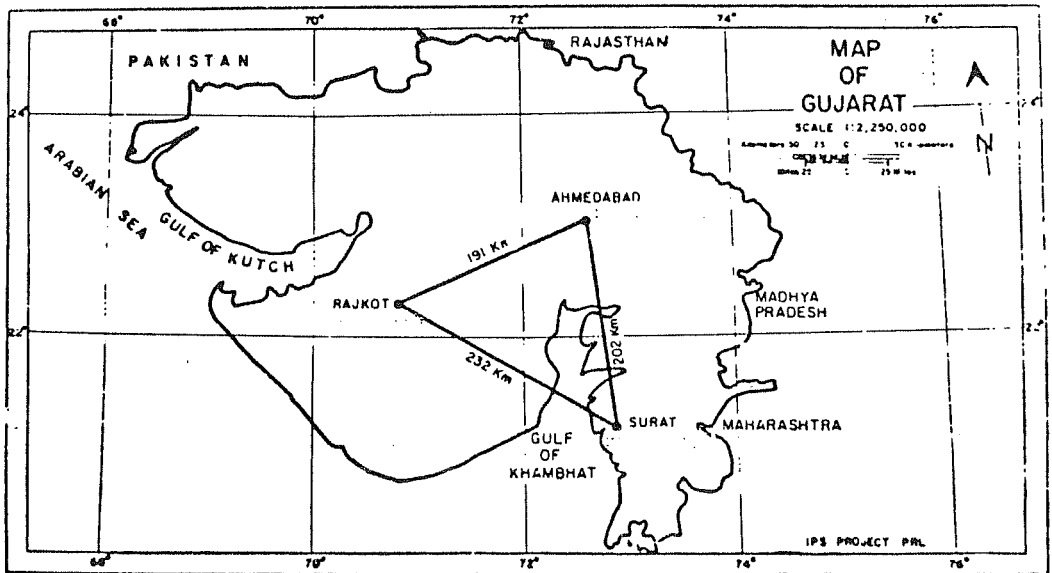


Fig. 3.1 Locations of three IPS stations in India. These stations form a 3-site solar wind observatory operating at 103 MHz.

- (ii) To estimate daily values of solar wind speed using the phenomenon of IPS of a number of radio galaxies.

The three R.Ts are located at Thaltej ($23^{\circ}02' 39''.48$ N, $72^{\circ}29' 38''.86$ E), Rajkot ($22^{\circ}17' 28''.82$ N, $70^{\circ}44' 26''.58$ E) and Surat ($21^{\circ}09' 05''.05$ N, $72^{\circ}47' 13''.30$ E) with base-lines measuring about 200 Km each (Fig.3.1). The telescopes are identical in all respects except that the antenna aperture of the Thaltej telescope was doubled in 1984 to measure approximately $10,000 \text{ m}^2$. This was done with a view to increase the sensitivity of the telescope to record weaker and hence larger number of scintillating sources. Systematic observations of these sources over the solar elongation range of 15° - 90° would then enable estimation of their angular sizes.

The work presented in this thesis is based on the IPS observations made using the Thaltej R.T. They comprise:

- (i) Enhanced scintillations of the radio source . PKS 2314+03 when it was occulted by the plasma tail of the Halley's comet;
- (ii) Displacement of intensity pattern produced by large-scale plasma density irregularities; and
- (iii) Scintillations of the compact source PSR 0531+21 in the Crab Nebula.

3.2 Basic Consideration for the design of the IPS Telescope

In designing this IPS telescope, the following important features were considered :

3.2 (a) Frequency of Operation

The principal consideration for the choice of the operating frequency of a radio telescope depends upon the scientific information one wants to extract. The choice of the operating frequency for IPS is made on the basis of the following facts:

- (i) IPS is a meter-wave phenomenon so that scintillations are inversely proportional to the operating frequency.
- (ii) The upper limit of frequency is set by the fact that at higher frequencies (> 300 MHz) the system (receiver) noise dominates.
- (iii) At lower frequencies the galactic background noise becomes prominent, and at frequencies below about 10 MHz, the ionosphere becomes opaque to the radio frequencies. Thus, a frequency in the range of 80-120 MHz is appropriate for IPS observations. The frequency of

103 MHz was, therefore, chosen for the three R.Ts.

The other IPS observatories in U.K., U.S.A., Japan and U.S.S.R. are working at frequencies of 81.5 and 151.5 MHz, 74 MHz, 327 MHz and 102.5 MHz respectively. At these mostly VHF frequencies IPS observations can be made over a solar elongation range of about 5° - 140° .

3.2(b) Size of the Telescope

The choice of the aperture of the IPS antenna array is made on the basis of the scientific objectives aimed at. Primarily with the emphasis on studying the density structure and dynamics of the solar wind over a wide range of ecliptic latitudes and solar elongations, it is necessary to observe a good number of scintillating radio sources around the Sun. With an aperture of about $3,000 \text{ m}^2$ at 74 MHz, the UCSD group observed 8-10 sources (Armstrong and Coles, 1972), whereas with $2,000 \text{ m}^2$ aperture at 69 MHz the Toyokawa group observed 4-6 scintillating sources (Watanabe and Kakinuma, 1972). With their new system at 327 MHz (Kakinuma and Kojima, 1984) observe 15 sources regularly. It was proposed to observe about 20-25 sources round the year in

order to study some of the characteristics of the IPM with an antenna aperture of about $5,000 \text{ m}^2$ at 103 MHz. The three R.Ts were therefore developed with antenna apertures of $5,000 \text{ m}^2$ each.

In March-April 1984, the aperture of the Thaltej antenna was doubled to $10,000 \text{ m}^2$ by extending the original antenna in the eastward direction. This has increased the sensitivity of the telescope so that radio sources with flux density of about 6 Jy can be recorded with a S/N of 5 with a receiver band-width of 2 MHz and integration time-constant of 0.1 sec.

3.2(c) Design Consideration of IPS Antenna Array

The number of scintillating radio sources which can be detected by a given R.T. depends mainly on:

- (i) Its declination coverage and effective antenna aperture together with receiver parameters, such as r.m.s. fluctuations in the receiver output, (ΔT_{rms}) , and
- (ii) minimum detectable flux density, (ΔS_{min}) or sensitivity of the telescope. Furthermore, the S/N for the scintillating flux of a source must be considered.

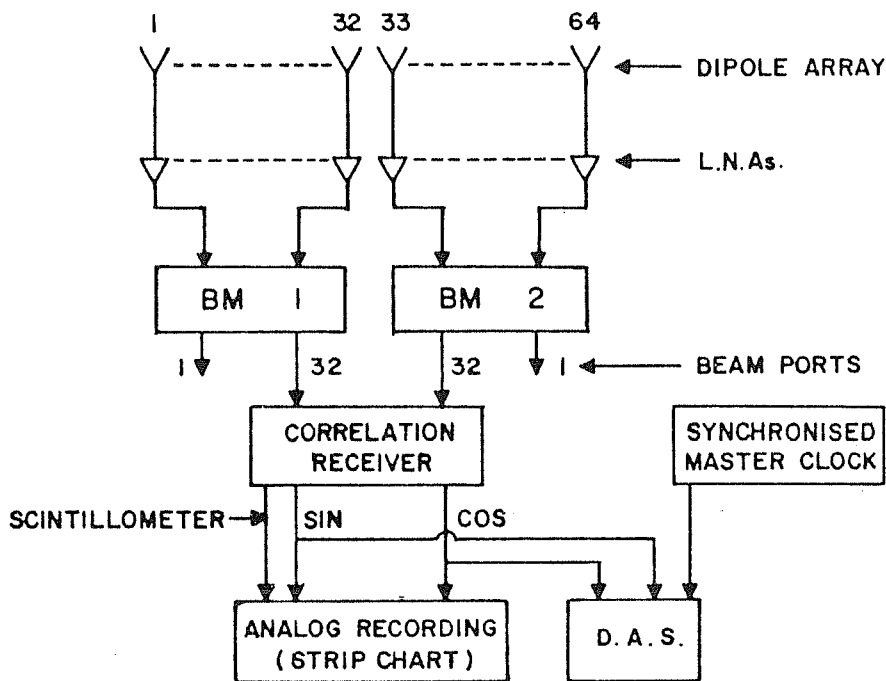
One of the ways by which IPS of a large number

of sources can be recorded would be to form a pencil beam of the antenna that can be steered electronically in the required directions. This would involve changing the phase gradients across the array in a pre-determined way and, therefore, would be quite inconvenient from operational point of view for long-term observations. Hence, it was decided to deploy a large number of beams in the sky once for all and let the Earth's rotation do the scanning, allowing for sufficient time for IPS observations on each source. From this one can select interference free observations for estimating IPS spectra, scintillation indices and from three-site data, solar wind velocities.

When all these requirements were put together, it was thought that they would be fulfilled by a fullwave dipole array. The concept of a multibeam-forming matrix seemed to be a suitable choice for scanning a large portion of the sky using 32 beams simultaneously. Thus, a fullwave dipole array, in conjunction with Butler matrices (Butler, 1966), constituted the multibeam antenna array.

The Thaltej array (after doubling) consists of 2048 fullwave dipoles connected in 64 East-West rows of 32 dipoles each forming a rectangular aperture measuring about 200 meters in North-South and 50 meters in East-West. This is followed by low-noise preamplifiers installed on the antenna poles to compensate mainly for the RF coaxial cable attenuation and insertion loss of the Butler matrices ahead of them

BLOCK DIAGRAM OF IPS TELESCOPE AT THALTEJ



DAS = DATA ACQUISITION SYSTEM
 BM = BUTTER MATRIX
 L.N.A. = LOW NOISE AMPLIFIER

Fig. 3.2 Block diagram of one of the IPS stations

3.3 The Radio (IPS) Telescope at Thaltej

Fig. 3.2 shows block diagram of Thaltej Radio (IPS) Telescope. (Sometimes it is also referred as Radio telescope at Thaltej.) The entire IPS telescope system can be divided into the following sub-systems:

- (a) Antenna array
- (b) Pre-amplifiers and multibeam-forming matrix
- (c) Receiver and analog data recording system
- (d) A/D conversion and digital data recording system.

3.3(a) Antenna array

Fig. 3.3 shows bird's eye view of part of the antenna. There are 64 rows of open wire transmission lines in E-W plane. Each transmission line consists of fullwave dipoles in N-S plane. The distance between each successive E-W row is 0.85λ . The separation between the parallel wires of transmission lines is 5 cm. This spacing of 5 cm, corresponding to the characteristic impedance of 400 Ohms, is maintained constant along the transmission lines by placing Hylem spacers at regular intervals of half wavelength.

The distance from the "short" on the transmission line to first dipole is $\lambda/4$. Thereafter, the distance between consecutive dipoles is $\lambda/2$. After the 16th dipole, there is another short at a distance of $\lambda/4$ on the other end of the transmission lines. Alternate dipoles are



Fig. 3.3 Bird's eye-view of a portion of Thaltej antenna. Transmission lines, reflecting wires and low-noise amplifier boxes are seen in this figure.

transposed to add the antenna currents in phase. Fig. 3.4 shows the schematic of a part of the antenna. All the dipoles are crimped on the transmission lines with the help of copper tees. 0.22λ below the plane of the transmission lines and the dipoles, there is a reflecting plane of copper-clad steel wires parallel to the dipoles. The spacing between these successive wires is $\lambda/10$.

In March-April 1984 the aperture of this antenna at Thaltej was doubled to $10,000 \text{ m}^2$ by extending the original antenna in the E-W direction (Fig. 3.4). The two parts of antenna are joined by an open-wire transmission line 1λ long having a characteristic impedance of 400 Ohms approximately. The feed point is taken from the centre of the connecting transmission line through a balun to the input of pre-amplifiers. In Fig. 3.4 dipole array denoted by 1 to 16 belongs to the old antenna while from 17 to 32 to the new one.

3.3(b) Pre-amplifiers and multibeam-forming matrices

In order to realise the maximum aperture sensitivity of the IPS antenna array, low noise pre-amplifiers were introduced after the baluns (matching system) (Fig. 3.4). The system temperature (Kraus, 1966), is given by:

$$T_{\text{sys}} = T_{\text{sky}} + T_{\text{R}} \quad \dots(3.a)$$

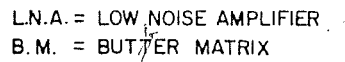


Fig. 3.4 Schematic of Thaltej IPS antenna.
Transmission lines and fullwave dipoles
are in E-W and N-S directions respectively.

where $T_R = (N-1) T_O$

T_{sky} = equivalent noise temperature of galactic background

T_R = noise temperature of receiver

N = noise factor of the pre-amplifier

and T_O = ambient temperature of the receiver.

At a frequency around 100 MHz, the sky background is about a couple of thousand degrees Kelvin (Kraus, 1966). Hence the sensitivity of the receiver becomes sky-noise limited. The pre-amplifiers, with a noise factor of about 2, are designed such that they selectively amplify (average gain 35 dB) the 103 MHz signal and compensate for the attenuation along the path to the receiver. Another important design consideration for the pre-amplifiers is their phase-stability. The RF signals amplified by the pre-amplifiers are fed into a multibeam-forming matrix. For good long-term phase-stability the band-width of an amplifier should be sufficiently large. The average band width (Half-power) of the pre-amplifiers is about 8 MHz.

To simplify the observation procedure of IPS of a number of radio sources, it was decided to operate the radio telescope as a transit instrument. Thus, instead of forming a pencil beam and switching it in different right ascensions and declinations (R.A.s and decs.) employing elaborate switching techniques, a steady multibeam pattern

can be formed using a passive beam-forming network, called a Butler matrix (BM). Apart from the ease of operation, the multibeam pattern of this device enables simultaneous scanning of equispaced strips of the sky when equal number of receivers are used. The envelope of the beams has a cosine taper such that the 16th beam will be nearly 3 dB down w.r.t. the beams near the zenith. Due to the N-S phasing, a 32-beam pattern results in declination for each of the North and South halves of the antenna.

Such a multi-strip scanning telescope would be particularly convenient for a radio sky survey and study of heliospheric disturbances related to geomagnetic activity (Gapper et al. 1982), using a new technique of producing "g-maps" of plasma turbulence (Hewish and Duffett-Smith, 1987).

The signal from a scintillating radio source is often very weak compared with the undesirable noise in the telescope. Even small changes in the level of this noise can mask those produced by the signal from the radio source. If a total-power receiver is used, it must be very stable. Such stringent stability conditions are not necessary for a correlation receiver. This telescope works as a correlation interferometer in conjunction with a correlation receiver so that its output is proportional to the time-averaged product of the voltages from the North and South halves of the antenna. Such a receiver is insensitive to most of the undesirable noise which normally

contributes only to the uncorrelated voltage components received from the two parts of the antenna, whose time-averaged product tends to zero.

Low-noise Pre-amplifier at 103 MHz

Fig. 3.4 shows the schematic arrangement of the array with low noise pre-amplifiers (LNA) and two multi-beam-forming matrices. The RF signal at 103 MHz from each EW row of 32 dipoles of the array is enhanced by a 3-stage LNA of the cascade type. In the second stage a gain-control is incorporated, so that the relative gain and phase of all the amplifiers are made identical as measured from inside the receiver room.

Butler Matrix at 103 MHz

Amplified RF signal is carried through the underground (3 ft. deep) coaxial cables to the BMs in the recording room. This ensures the gain and phase stability of the signal which are the pre-requisites of the BMs. The 64 coaxial cables carrying 64 independent amplified outputs of the entire array are divided into two equal groups, one from the first 32 cables (Northern half) and other from the remaining 32 cables (Southern half). Using a combination of a standard signal generator and a precision RF vector voltmeter, it was ensured that a given 103 MHz signal at the input ports of the pre-amplifiers arrived at these cable ends with very small relative amplitudes

(within ± 0.5 dB) and phases (within $\pm 1.5^\circ$). Using a Butler matrix, a multibeam pattern is formed once for all, so that each of the beams points in a particular declination. A Butler matrix generates simultaneous independent beams from identical outputs of an array with a uniformly illuminated aperture (Butler, 1966). The important theoretical considerations for this device are the following:

For an 'n' element linear array, the normalised magnitude of the field intensity in the far-field is given by (Kraus, 1966)

$$E = \frac{1}{n} \frac{\sin (n \psi / 2)}{\sin (\psi / 2)} \quad \dots (3.b)$$

where $\psi = \frac{2 \pi}{\lambda} d \sin \alpha - \delta$

d = element spacing

λ = wavelength

α = angle from the array normal

δ = element-to-element phase shift

If K is the beam number, the element-to-element phase shift for the K^{th} beam is given by (Delaney, 1962)

$$\delta k = \frac{(2K-1)\pi}{n} \quad \dots (3.c)$$

The normalized far-field amplitude of the K^{th} beam, when hybrid rings are used, is

$$|E_k| = \frac{1}{n} \cdot \frac{\sin(n\pi d/\lambda) \sin(\alpha) - (k\pi)}{\sin(1/n) \sin(n\pi d/\lambda) \sin(\alpha) - (k\pi)} \cdot \cos(\pi/2 \sin(\alpha))$$

...(3.d)

E_k = Normalized magnitude of far field-intensity of K^{th} beam

n = Number of elements in the array

λ = Operating wavelength

d = Element-to-element spacing

K = Beam number

α = Angle from array normal

$\cos[\pi/2 \sin(\alpha)]$ is called the array factor.

The peaks of various beams occur at values of the angle α which make the numerator and denominator of eqn. (3.d) equal to zero. Denoting these angles by α' , we get

$$\sin \alpha' = \frac{\lambda}{nd} (nq + K - \frac{1}{2}) \quad \dots(3.e)$$

where $q = \text{An integer}$

For $q = 0$, Eqn. (3.e) gives the positions of main beams
and For $q \neq 0$, it will give the positions of grating lobes

The angular coverage θ of multibeam pattern is
given by

$$\theta \approx 2 \sin^{-1} \left[\lambda/2d \left(1 - \frac{1}{n} \right) \right] \quad \dots(3.f)$$

For large arrays where $n \gg 1$

$$\theta \approx 2 \sin^{-1} (\lambda/2d) \quad \dots(3.g)$$

Thus, for large arrays the angular span depends only
on wavelength and inter-element spacing.

Computer plot of the multibeam pattern in declination for a 32-element BM is shown in Fig. 3.5. Each beam has a size to half power of about (3.6° EW x 1.8° NS) at zenith and realizes the gain corresponding to the aperture size. The adjacent beams cross each other at (-4dB) points. At the wavelength of 2.91 meters and element-spacing of 0.85λ , the angular coverage in declination of the pattern works out to about $\pm 30^\circ$ around the zenith. The overall bandwidth of the matrix was measured to be about 2% of the

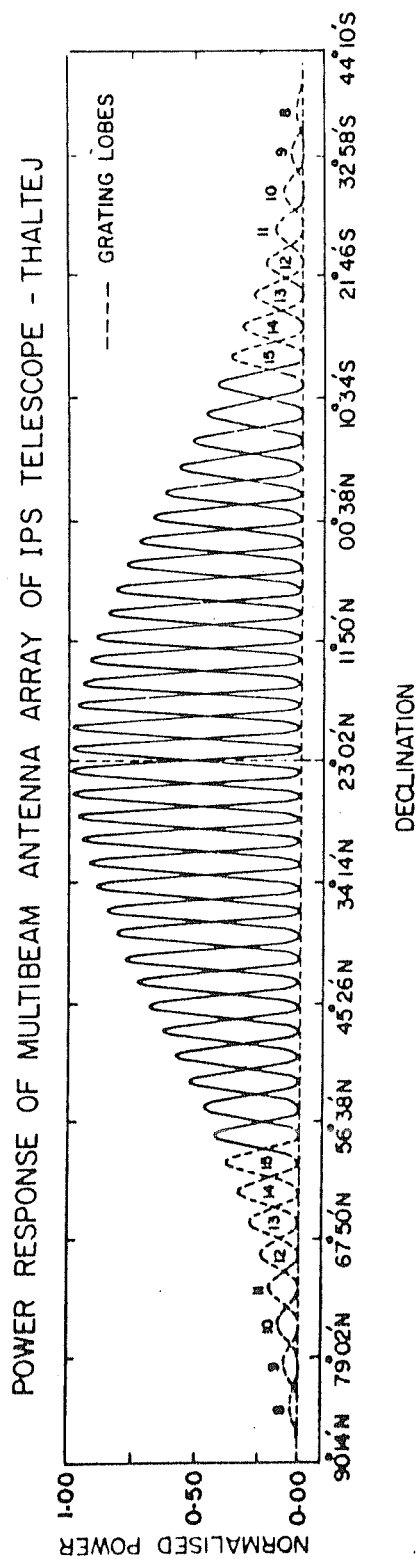


Fig. 3.5 Computer plot of the multibeam pattern in declination for a 32-element Butler Matrix. Each beam has a size to half power of about $(3.6^\circ \text{ EW} \times 1.8^\circ \text{ NS})$ at zenith.

centre frequency of 103 MHz.

Due to the foreshortening effect resulting from the apparent change in the inter-element spacing of the antenna array (Kraus, 1966), grating lobes are formed when the main lobe of the antenna is pointed in a direction away from the zenith. Grating lobes become important beyond the 12th beam (Fig.3.5) on either side of the local zenith. Observations made with beams 10th (on either side of the local zenith) and beyond should, therefore, be interpreted with caution.

3.3(c) Receiver and Analog Data Recording System

Fig. 3.6 shows a block diagram of the correlation receiver. It is a dual channel receiver (SIN and COS) which is connected to the two halves of the antenna array to form a phase-switched interferometer in declination. The receiver has a common crystal-controlled local oscillator operating at 73 MHz, giving an IF of 30 MHz for each channel with a bandwidth of about 2 MHz. The effective noise figure of the system is quite low, limited only by the galactic background, as low noise pre-amplifiers are used immediately after each antenna array.

In this IPS telescope a correlation receiver is used. In such a receiver, the IF output voltages from two identical receiver channels are multiplied. Consequently, time-averaged uncorrelated noise voltages produce zero d-c voltage at the multiplier output. A compact

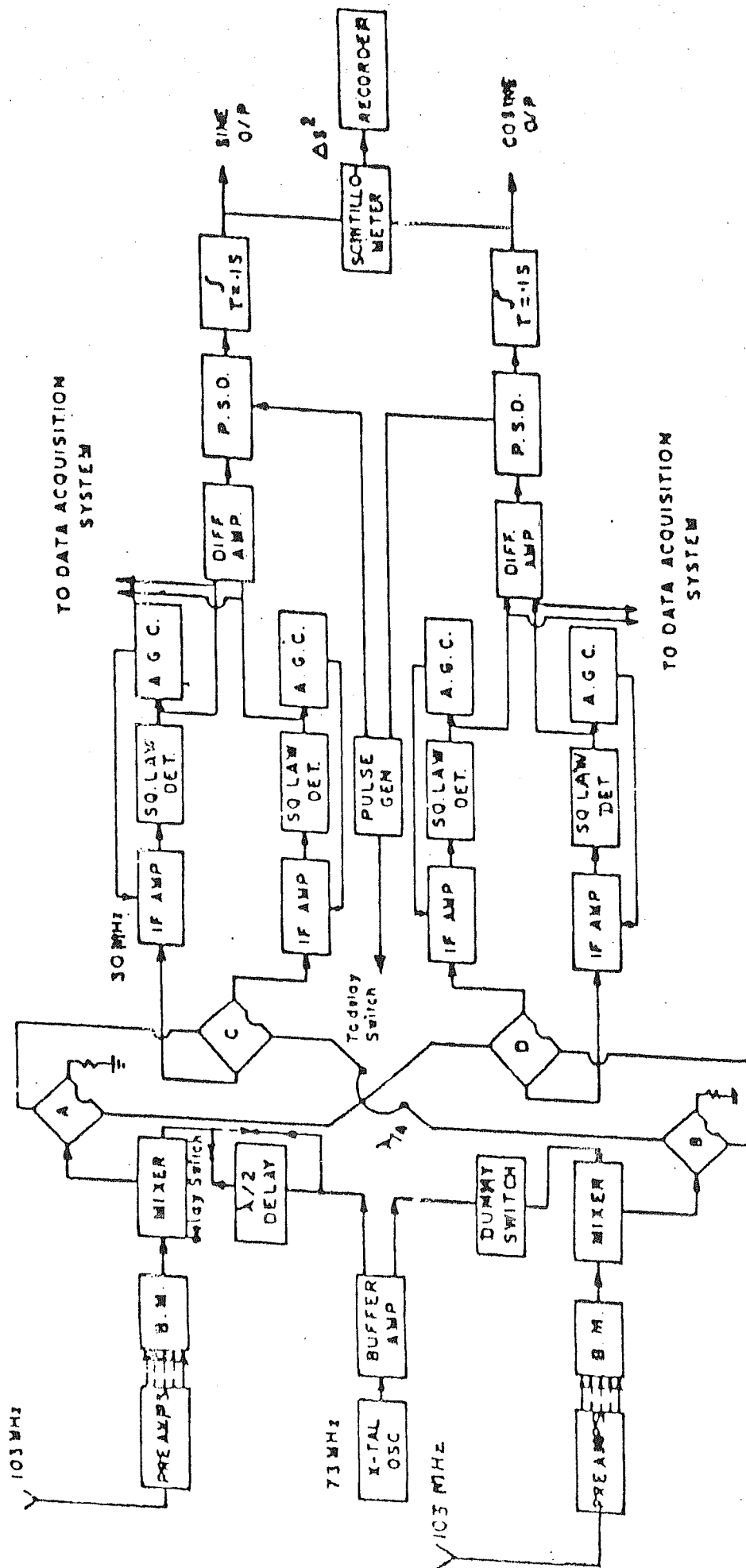


Fig. 3.6 Block diagram of correlation receiver used at Thaltej.

radio source will produce correlated signal power (equal to $k\Delta T B$) at the inputs of the receiver and IF output voltages having outputs proportional to $(k\Delta T B)^{\frac{1}{2}}$, where k is the Boltzman constant, ΔT is the change in the noise level due to the radio source and B is the pre-detection bandwidth. If the phase difference between them is ϕ the dc output voltage of the multiplier becomes $k.\Delta T.B \cos\phi$.

The sensitivity or minimum detectable temperature of the correlation receiver is given by (Kraus, 1966)

$$\Delta T_{\min} = \frac{1}{\sqrt{2} \cos\phi} \frac{T_{\text{sys}}}{\sqrt{B \cdot \tau}} \quad \dots(3.h)$$

where τ is the post-detection integration time constant. For $B = 2$ MHz and $\tau = 0.1$ sec. and assuming $T_{\text{sys}} \approx 2000^\circ\text{K}$, ΔT_{\min} turns out to be $\sim 3.5^\circ\text{K}$

Therefore, the minimum detectable flux, which is defined as $\Delta S_{\min} = \frac{2k \Delta T_{\min}}{A_{\text{eff}}}$ where A_{eff} is effective area of the antenna, turns out to be about 6 Jy with S/N of 5 for $A_{\text{eff}} = 8000 \text{ m}^2$.

Signals from the two halves of the antenna array are brought to two identical 32-element beam-forming matrices BM-1 and BM-2. For a given source, signals from the corresponding beam ports are given to the inputs of the receiver through low-noise pre-amplifiers of the type

described earlier. A common local oscillator (73 MHz) feeds the two balanced mixers through a phase switch. The outputs of the two mixers are each divided into two parts using coaxial hybrid rings A and B as power dividers. Output signals from A and B hybrids are combined in phase in the third hybrid D for COS signals, while the second output from A is combined in the fourth hybrid C with the second output from B after a delay of 90° . The output of C, therefore, gives the SIN signals. Each of the two receiver channels has two 30 MHz intermediate frequency (IF) amplifiers with an average bandwidth (to half power) of about 2.0 MHz. The outputs of these high gain (80 dB) IF amplifiers are maintained at a constant level within about 1 dB using automatic gain control (AGC) having a time constant of about 3 seconds. The range of the square-law detectors is -35 to -8 dBm.

Low-pass filtering of 0.1 sec has been used after the phase-sensitive detectors (PSD). This integration time-constant therefore, allows intensity fluctuations upto a limit of 10 Hz. Ionospheric scintillations, which are expected to be weak at tropical latitudes at 103 MHz when present, are prominent below about 0.1 Hz. The IPS data are, therefore, passed through a digital filter with a low frequency cut-off at 0.1 Hz before computing the IPS spectra.

The square-law detector diodes are selected for similarity and are connected in such a way that the output

voltage remains within the square-law range of 5-70 mV. The AGC is so adjusted that with the antenna array connected, but no source in the beam, the square-law output remains below 45 mV.

For uncorrelated signals the output of the difference amplifiers remain zero. Correlated signals produce output voltage at COS or SIN channel or at both, depending on the relative phase of the input signals. This square-wave modulated signal at the switching frequency is converted to sine-wave by the active filter-circuit and phase-detected in synchronisation with the phase switch.

The SIN and COS outputs are recorded on a chart recorder as well as on a digital tape recorder after A/D conversion at 20 times/sec. The response of a phase-changing interferometer to a scintillating radio source comprises three components (Duffett-Smith, 1976):

- (i) A broadband system noise voltage
- (ii) A slowly-varying voltage due to the passage of the source through the interference pattern of the telescope. The upper limit of its frequency spectrum is given by $7.3 \times 10^{-5} (d/\lambda) \cos \delta$ Hz, which works out to about 1.2×10^{-3} Hz for $\delta = 0$ for the Thaltej telescope. Here 'd' is east-west dimension of the antenna, ' δ ' is the declination and ' λ ' is the operating wavelength.

- (iii) A rapidly changing voltage caused by the scintillations, it has a noise like character and its frequency spectrum depends on the existing conditions in the solar wind, solar elongation, the apparent angular diameter of the source, the receiver bandwidth, etc.

The scintillating signals at the outputs of the SIN and COS receivers may be expressed as (Duffett-Smith, 1976)

$$V_S = f(t) \cdot A \cdot \sin(bt) \cdot \frac{\sin^2(at)}{(at)^2} \quad \dots(3.i)$$

and
$$V_C = f(t) \cdot A \cdot \cos(bt) \cdot \frac{\sin^2(at)}{(at)^2} \quad \dots(3.j)$$

where $A \cdot \sin(bt) \cdot \frac{\sin^2(at)}{(at)^2}$ and

$$A \cdot \cos(bt) \cdot \frac{\sin^2(at)}{(at)^2}$$

are the patterns of this slowly-varying voltage and the function $f(t)$ defines the temporal changes in its amplitude.

Scintillometer Unit

The SIN and COS signals are also fed to a scintillometer (Fig. 3.7). This unit squares the scintillating part of the two signals and adds them, averaging over a long time constant of 47 seconds. The scintillometer output shows a deflection proportional to the square of the scintillating flux, modulated by the square of the antenna pattern. The output is recorded on the third channel of the chart recorder along with the SIN and COS signals.

The sensitivity of the scintillometer is expressed (Duffett-Smith, 1976) as.

$$(\Delta S)_{\min} = 4 \frac{k \cdot T_N}{A_{\text{eff}}} \left[\frac{1}{\tau_1 \cdot \tau_2 \cdot \Delta f^2} \right]^{\frac{1}{4}} \quad \dots (3.k)$$

where, ΔS = r.m.s. value of the scintillating flux density of the source.

T_N = System noise temperature

A_{eff} = Effective antenna area, about $8,000 \text{ m}^2$ for IPS telescope at Thaltej.

τ_1 = 0.1 sec (time constant of SIN and COS integrators)

τ_2 = 47 seconds (time constant of scintillometer integration.

Δf = Overall (-3dB) bandwidth of the IF amplifiers $\approx (2 \text{ MHz})$.

TOTAL-POWER SQUARING SCINTILLOMETER

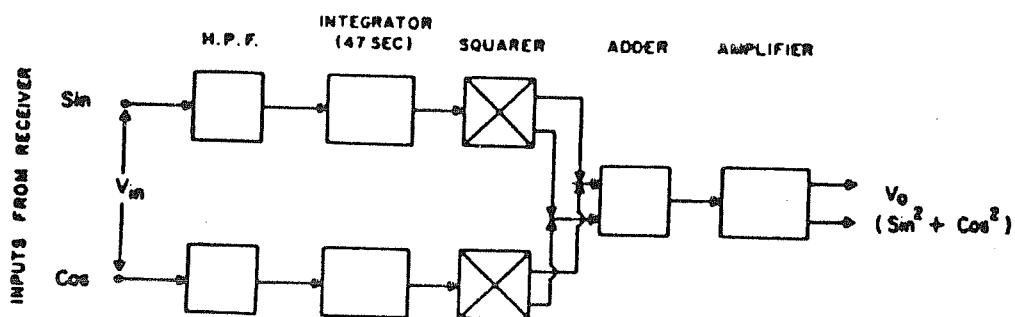


Fig. 3.7 Block diagram of scintillometer unit at Thaltej.

For the Thaltej R.T. scintillometer, the sensitivity turns out to be about 1.0 Jy r.m.s. ($1 \text{ Jy} = 10^{-26} \text{ W m}^{-2} \text{ Hz}^{-1}$).

3.3(d) A/D conversion and digital data recording system

The SIN, COS and scintillometer outputs are recorded on a 3-channel strip-chart recorder for the purpose of monitoring the quality of the IPS observations. The SIN and COS data are simultaneously converted into digital form and recorded on magnetic tapes for further processing and analysis.

The data available from the correlation receiver have a band-limited spectrum upto about 10 Hz (IPS spectrum lies between about 0.1 Hz to 10 Hz). The simple integrator serves the purpose of a low-pass filter. No special hardware filter is used. The two receiver channels have outputs whose magnitudes depend on the source position (declination) on the receiver fringe of the interferometer formed by the North and South halves of the antenna array (Fig. 3.5). At any time, one may get the output in SIN and/or COS fringe, as well as the corresponding scintillometer output.

Fig. 3.8 shows a block diagram of the data acquisition system (DAS) indicating most of the inputs/outputs (I/O) signals. The system is divided into the following sub-systems:

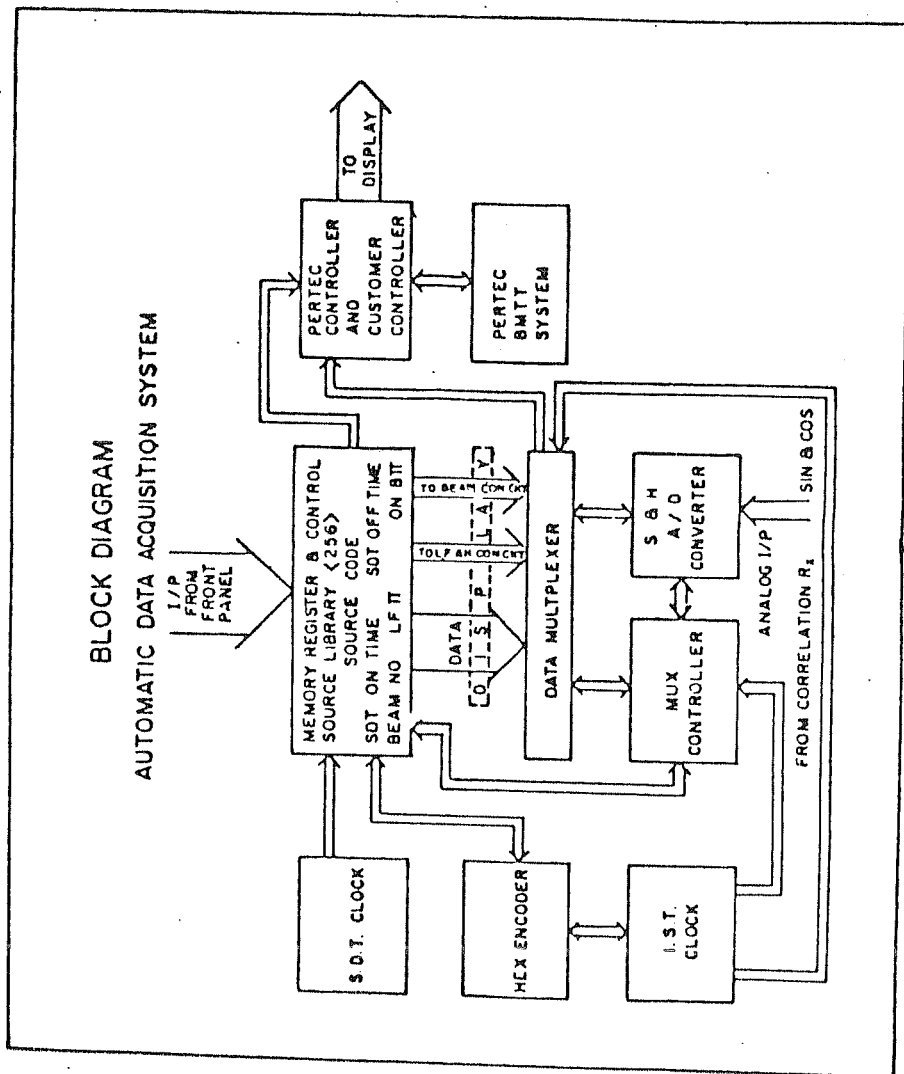


Fig. 3.8 Block diagram of data acquisition system.

- (i) Source library
- (ii) Hex Encoder
- (iii) Control Circuit
- (iv) A/D Converter
- (v) Data Multiplexer
- (vi) MUX Controller
- (vii) Pertec Controller

The system keeps track of a sidereal clock (SDT) and decides about various observing schedules to be followed to an accuracy of a minute. This avoids up-dating the transit time by 4 minutes every day. Once the SDT is stored for a source in the source library, it is unaltered throughout the observing session.

3.4 Calibration

For reliable and precise results, periodic calibration of the telescope is very essential. One should be able to estimate the mean flux, \bar{S} and the scintillating flux, ΔS of a scintillating radio source observed by the telescope. This, in turn, will help in the calculation of several other useful parameters regarding the radio source and the intervening medium.

The R.T. at Thaltej was calibrated by observing a number of radio sources of medium flux density. The radio sources used were - 3C 47, 3C 71, 3C 84, 3C 123, 3C 175, 3C 273, 3C 286, 3C 287, 3C 454.3, 3C 457, 3C 459

and 3C 465. To know the average response, several (typically five) observations were made. The response of each source was monitored on a strip-chart using the SIN and COS channels from which deflections D_s and D_c respectively were noted (Fig. 3.9a).

The effective response, $D_{\text{eff}} = (D_s^2 + D_c^2)^{\frac{1}{2}}$ was calculated for each observation of the source. Then the average of all the D_{eff} was calculated. The mean fluxes (dc) of the sources were extrapolated from the flux values available for these sources at 81.5 MHz (Readhead and Hewish, 1974). Flux at 103 MHz was estimated by using $S_f \propto f^{-0.75}$, where f is the operating frequency. A best-fit line was drawn through the data points, using the least-squared law, Fig. 3.10.

The scatter seen in this plot could be due to the fact that different sources pass through their respective beams at different levels of sensitivity. Also, any variations in the behaviour of the overall R.T. system enhances the scatter.

As one moves on either side of the local zenith beam, the gain of the antenna reduces according to the envelop of the antenna multibeam pattern Fig. (3.5) described earlier. Deflections obtained from this plot were corrected for the envelop of the beam pattern.

From Fig. 3.10 of 'System calibration' it is seen

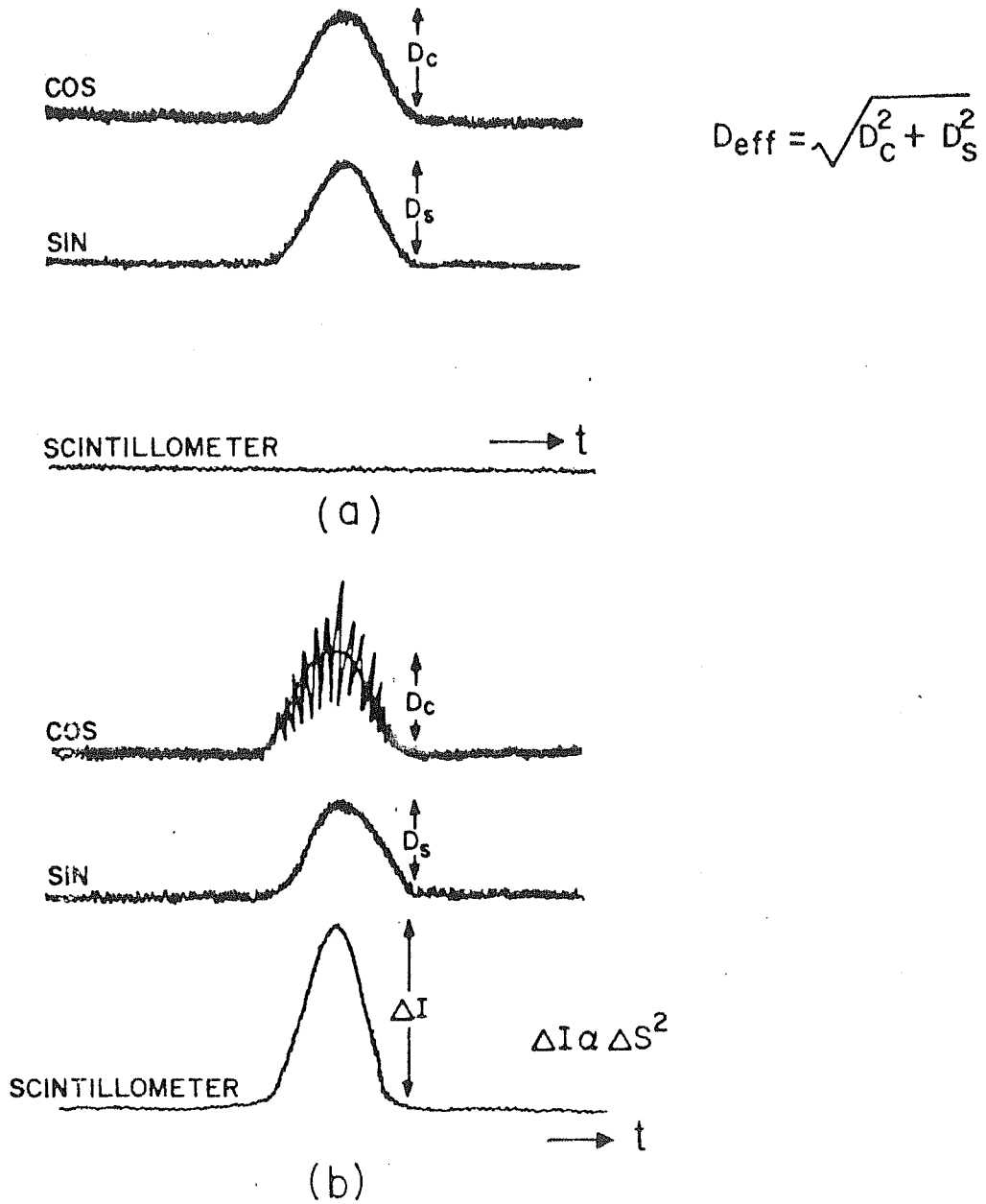


Fig. 3.9 Strip chart recording when there is (a) non-scintillating (b) scintillating source in the beam.

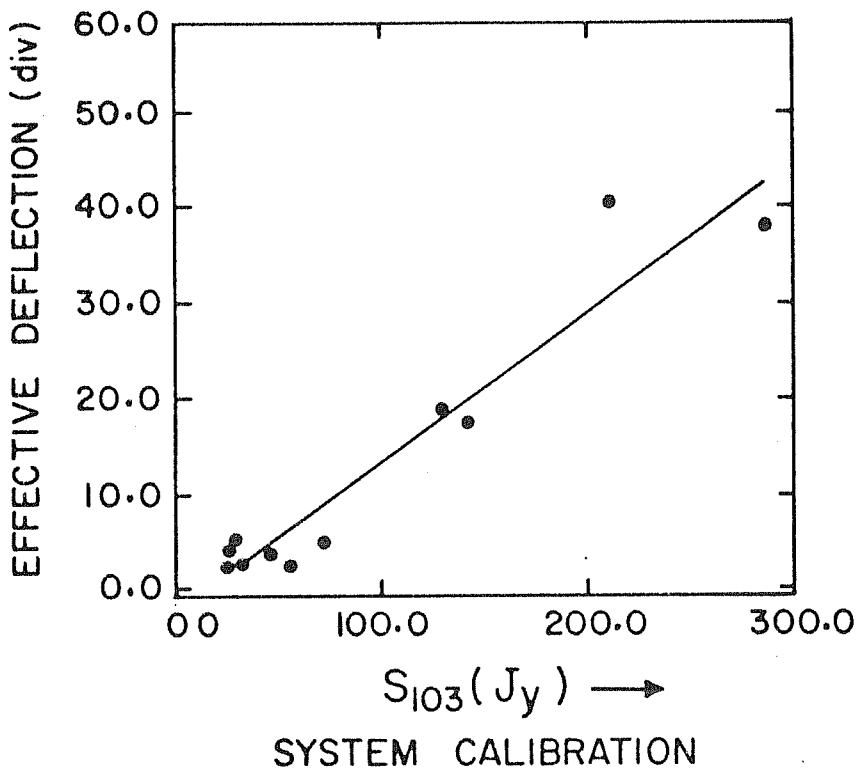


Fig. 3.10 Effective deflection vs. flux at 103 MHz. Each point is an average of many observations of calibrating sources. Solid line is a least-squared fit to the data.

that the slope,

$$m = \frac{D_{\text{eff}} (D)}{\text{Flux} (S)} = 0.16 \pm .047 \quad \dots(3.a)$$

The change in the flux of the source, ΔS , will cause the deflection (response) to change. Hence, eqn. (3.a) can be written as

$$\Delta S = \frac{\Delta D}{m} \quad \dots(3.b)$$

For the measure of scintillation, the scintillometer should also be calibrated to estimate the scintillating flux of a radio source.

The scintillometer calibration was carried out by using a function generator (FG), (or a noise generator). An input signal in volts, v_i from the FG at 8 Hz was provided to the SIN and COS channels simultaneously using an ISO-T. This input was increased in steps of 0.1 volts and the corresponding outputs v_o were noted. Fig. 3.11 shows the logarithmic plot of v_i vs. v_o . The slope of this plot is about 2 which verifies that the scintillometer follows a square-law; i.e.

$$v_o \propto v_i^2 \quad \dots(3.c)$$

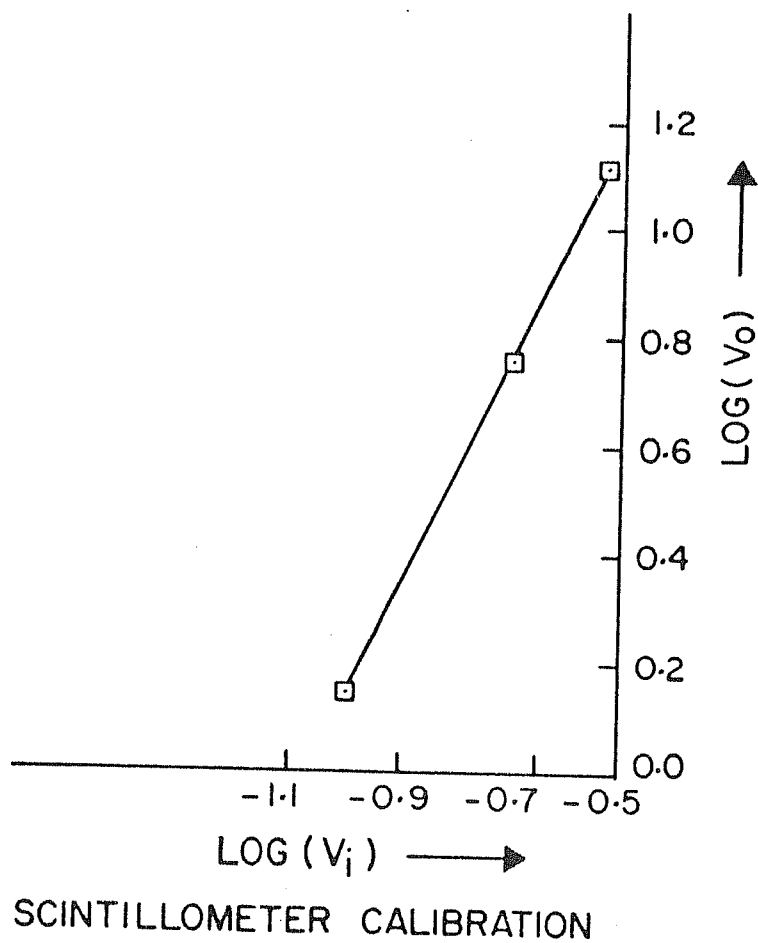


Fig. 3.11 Logarithm plot of input output of scintillometer in volts.

Any change in the input signal causes the corresponding change in SIN and/or COS channel deflection. In the case of a scintillating source, in addition to deflection in the SIN and/or COS channels, the scintillometer output shows a deflection proportional to the square of the scintillating flux of the source. Thus, the change in intensity ΔI , due to the scintillating flux is expressed as

$$\Delta I \propto (\Delta D)^2 \text{ (as scintillometer follows the square-law)}$$

$$\text{or } \Delta I = K (\Delta D)^2 \quad \dots(3.d)$$

On making use of the eqn. (3.b), eqn. (3.d) can be rewritten as

$$\Delta I = K (m \Delta S)^2$$

$$\text{or } \Delta S = \frac{1}{m} \sqrt{\frac{\Delta I}{K}} \quad \dots(3.e)$$

where ΔS is the scintillating flux of a source and ΔI is its deflection, m is the slope of the best-fit line of the system calibration of Fig. 3.10 and the proportionality constant 'K' can be found from the Fig. 3.11 of scintillometer calibration.

Taking the logarithm of eqn. (3.d), we get

$$\log \Delta I = \log K + 2 \log \Delta D$$

On comparing this eqn. with the eqn. of a straight line $Y = mx + C$, one gets

$$Y = \log \Delta I \text{ or } Y = \log v_o \text{ [as } \Delta I \propto v_o \text{]}$$

$$m = 2, X = \log \Delta D \text{ or } X = \log v_i \text{ (as } \Delta D \propto v_i \text{)}$$

and $C = \log K$ (intercept on Y axis in Fig. 3.11)

$$K = \text{Antilog (intercept)}$$

Fig. 3.11 gives the value of K to be about 10.

$$\Delta S = \frac{1}{0.16} \sqrt{\frac{\Delta I}{10}} \text{ Jy}$$

$$\approx 2 \sqrt{\Delta I} \text{ Jy} \quad \dots(3.f)$$

(ΔI can be read as in Fig.(3.9b))

Therefore, by knowing the scintillometer deflection ΔI from the strip-chart^{*}, one can calculate the scintillating flux. For background (Fig. 3.9b) when there is no source in the beam this

$$\Delta S \approx 1.2 \text{ Jy} \quad \dots(3.g)$$

This is the value one would get even if there is a non-scintillating source in the beam.

* Full-scale deflection on the strip chart i.e. 100 small divisions correspond to 10 volts.

Such calibrations were carried out quarterly and the system performance was found nearly steady.

3.5 Specifications of the Radio telescope at Thaltej

Coordinates of the site

Longitude 72° 29' 38".86 E

Latitude 23° 02' 39".48 N

Antenna

Type	:	Filled-aperture fullwave dipole array.
Frequency	:	103 MHz
Band allocated	:	103 ± 1.5 MHz
Polarization	:	North-South (Horizontal)
Configuration	:	North and south half antenna responses multiplied forming interferometer in declination. Each half comprises 32 E-W rows each of 32 dipoles connected by an open-wire transmission line formed into a cavity feeder.
Reflector-screen	:	A plane reflector-screen installed about a quarter wavelength below the dipoles, consists of copper-weld/galvanized steel wires, running North-South with East-West separation of a tenth of the operating wavelength (2.91 m)

Physical area of the antenna array : About 10^4 m^2

Effective area of the antenna array : about $8 \times 10^3 \text{ m}^2$

Gain : 41 dB

Beam width (at half power) : $3.6^\circ \times 1.8^\circ$ (at the zenith)

Impedance at each antenna array unit : 50-60 Ohms \pm 3 pF average

VSWR on the transmission line : 2:1 average

Preamplifiers

Centre frequency : 103 MHz

Band width (-3dB) : 7 MHz (average)

Gain : 30-40 dB

Noise Figure : 3 dB average

Input and Output impedance : 55-60 Ohms \pm 3 pF

Multi-beam forming matrix (Butler matrix)

Insertion loss : 1 dB

Phase error : 1.5° average and 4° in the worst case

Port impedance : 54 Ohms \pm 2 pF

Isolation between ports : 35 dB typically

Transmission linearity : 0.3 dB

Angular coverage of the beam pattern : $\pm 30^\circ$ of local zenith in declination

Angular separation between maxima of adjacent beams : about 2° (nominal)

Cross-over levels of beams relative to their maxima : - 4 dB

Grating lobes levels : 16th beam has an equally strong grating lobe located from the zenith about 35° on the other side of it.

Receiver

Type : 2-channel correlation receiver

Mode of operation : Phase-switching between responses of north and south halves of the antenna array.

Centre frequency : 103 MHz

I.F. frequency : 30 MHz average

AGC suppression range : I.F. I/P (-60 dBm)
O/P (46 mv) average
I.F. I/P (-30 dBm)
O/P (90 mv) average

TABLE 3-I

Correlation interferometer operating
as transit instrument

1. Operating frequency : 103 MHz \pm 1.5 MHz
2. Declination coverage : \pm 30° around local zenith
3. Pre-detection band : 2 MHz
width
4. Post-detection time : 0.1 Sec.
constant
5. Minimum detectable : 6 Jy
flux
6. System temperature : 2,000°K
7. Intermediate freq- : 30 MHz
uency

CHAPTER FOUR

ENHANCED SCINTILLATION OF A RADIO SOURCE CAUSED BY THE ION-TAIL OF THE COMET HALLEY

4.1 Introduction

Comets have been interesting objects for scientific studies since centuries. In ancient (pre-telescopic era) days only visual studies of comets could be made. With time, technology improved and further studies became practicable. Many comets visit inner solar system periodically and give us occasions to study them. In wavelengths other than radio, particularly in the optical and infra-red bands, much study has been made.

The nucleus of a comet, which has a typical size of

a few kilometers, is composed largely of ices (such as H_2O , CO_2 , etc.) mixed with dust (Whipple, 1950, 1955). When the comet approaches the Sun within ~ 3 AU, due to sunlight its ices are sublimated carrying with it the molecules and the dust. These form a coma of typical size of about 10^5 Km. When the comet further approaches the Sun within about 1 AU, the solar ultraviolet radiation dissociates and photoionizes the cometary molecules. These ions interact with the solar wind and move in the anti-solar direction. Indeed, the existence of the solar wind itself was postulated on the basis of observations of cometary ion-tail orientation (Biermann, 1951).

The solar wind moving away from the Sun at a typical speed of about 400 Km/s, carries with it the solar magnetic field. Due to the solar wind pressure, these magnetic field lines drape around the coma of the comet. The ionized particles from the coma follow these curved magnetic field lines and hence the formation of cometary ion-tail takes place (Alfven, 1957). Due to the polarity reversal of magnetic field lines at sector boundaries with a periodicity of about 7 days, detachment of the old and formation of new ion-tail takes place whenever a sector boundary crosses the tail. This process, called a disconnection event (DE), takes about couple of days to complete.

The comets have induced magnetic field due to comet-solar wind interaction (Alfven, 1957). A comet has two

types of distinctive tails. The first one is the ion-tail, having plasma phenomena and appears blue due to the emission lines of CO^+ . Typical extent of this tail is about 10^8 Km, oriented closely in the anti-sunward direction. The other tail is called the dust tail which appears yellowish-red in reflected light. The substructures visible in the ion-tail are in various forms such as rays, streamers, knots, kinks and filaments. Some of these features are caused through interaction with the solar wind (Jockers and Lust (1973); Ip and Axford (1982) and move in the anti-solar direction with velocities ^{of} about 20-200 Km/s. estimated from successive photographs of the tails.

To make meaningful observations, a comet should be periodic and bright. These criteria were fulfilled by the comet Halley, whose average periodicity is about 76 years.

For its 1985-86 apparition, various ground-based and space-borne observations were planned. During this apparition, the comet Halley was studied (in-situ) by various spacecraft, namely - Vega 1 and 2, Sakigake and Suisei, Giotto and the international cometary explorer (ICE). The missions had three main objectives - (i) to determine the dust content of the comet and distribution of particle sizes. (ii) to determine the nature and quantity of the material that make up the comet's nucleus and (iii) to study processes occurring in the coma and the interaction of the coma with the solar wind. Long awaited recent apparition

tion of the comet Halley was welcomed by the scinetists all over the world. For, this was one of the ideal comets for making observations of various features of its coma, dust and ion-tails. The P/Halley shows the full range of cometary activity (jets, halos, dust, ion-tails, etc.) and it also follows a predictable orbit.

Just as the small-scale density irregularities in the solar wind cause scintillations of compact radio sources, known as IPS phenomenon described earlier, it was thought possible that similar density irregularities in a fully developed cometary ion-tail of a strong comet might cause enhancement of scintillations, if the tail occulted a scintillating radio source. Towards this end an attempt was made by Ananthakrishnan et al. (1975), to observe the fluctuations in intensity of the compact source PKS 2025-15, at 327 MHz, when it was occulted by the comet Kohoutek (1973f) on 5 January 1974. They reported that no unique explanation could be given of the intensity fluctuations with 10 sec. periodicity in terms of scintillations produced by cometary plasma. However, Lee (1976) showed that these observations of Ananthakrishnan et al. (1975) could be interpreted as scintillations caused by the turbulent plasma in the comet's tail. In this way the ambiguity persisted for long time, of whether the plasma irregularities present in the cometary tail can cause scintillations or not.

The purpose of our observations of the occultation event in December 1985 was to decide whether the plasma

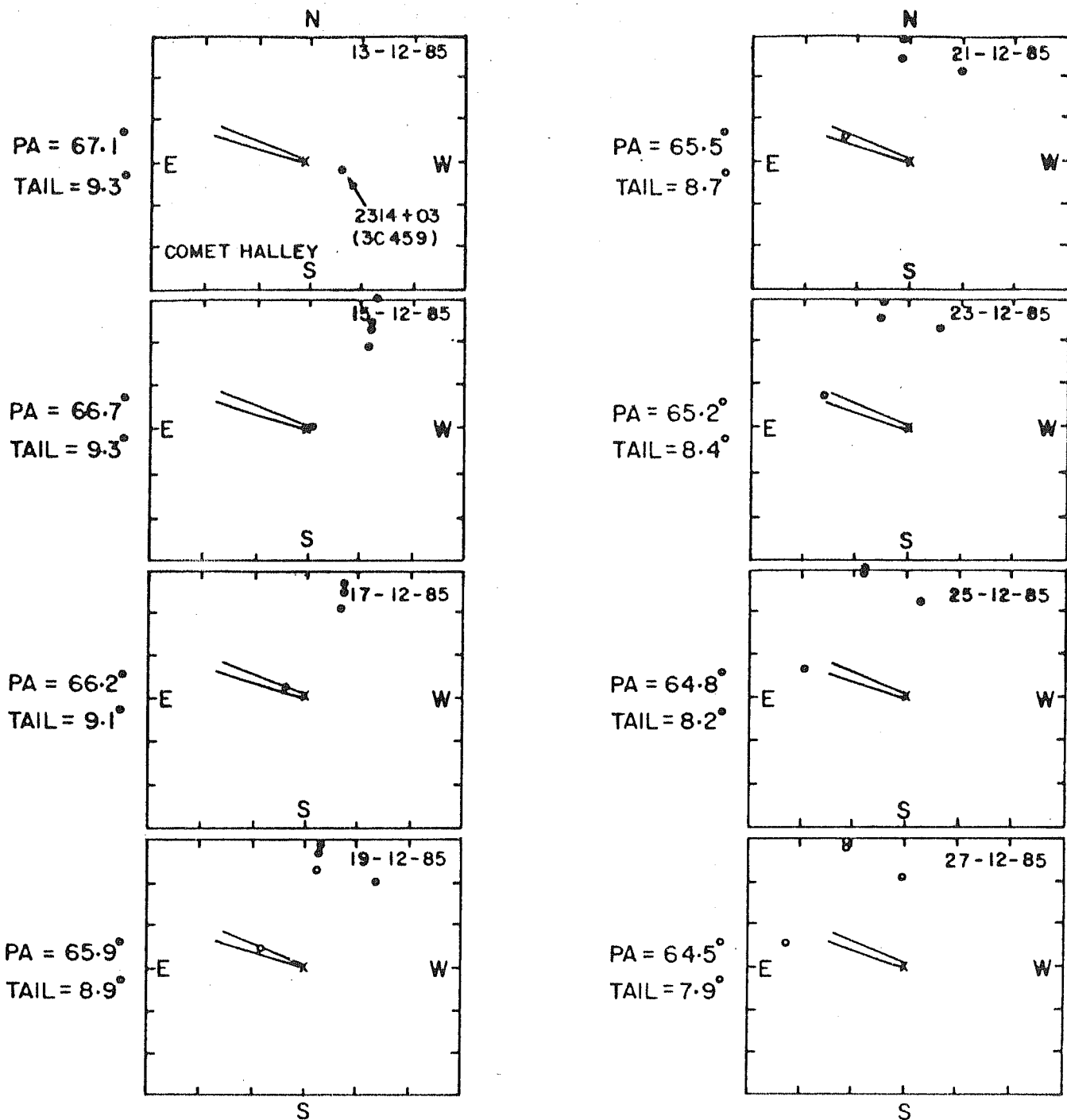


Fig. 4.1 Relative positions of PKS 2314+03 and Halley's Comet shown on alternate days from 13 through 27 December 1985. Note the occultation of the radio source by the cometary ion-tail during 18 through 20 December.

irregularities in the ion-tail can produce scintillations of a radio source. If yes, what were the densities of the plasma, plasma irregularities, their scale-sizes, etc.

4.2 Observations

Based on International Halley Watch (IHW) predictions, the quasar 3C 459 was to be occulted during 18-20 December 1985. Fig. 4.1 shows the relative positions of the quasar PKS 2314+03 (3C 459) and the Halley's comet as projected on the sky. The IPS telescope at Thaltej ($23^{\circ} 02' 39''.48$ N, $72^{\circ} 29' 3''.86$ E) near Ahmedabad was well-monitored and receiver calibrations were carried out periodically to ensure satisfactory performance of the telescope. Systematic observations of the occultation event were planned. To monitor the background scintillation level, regular observations of IPS of 3C 459, with $\sim 70\%$ of the total flux in the 0.45 arcsec component, were started right from 2 December 1985, when the solar elongation of the quasar was $\sim 103^{\circ}$. In addition, 5 other scintillating and non-scintillating radio sources were observed (viz. 3C 298, 3C 318, 3C 324, 3C 368, 3C 409), which were within 2° to 23° declination range of 3C 459, to have a check on ionospheric and interplanetary transient effects (Hewish et al. 1985).

Fig. 4.2, based on the parameters given in IHW newsletter No.7, shows schematically (not to scale) the geometry of the occultation of 3C 459 by the Comet Halley. Table 4.I,

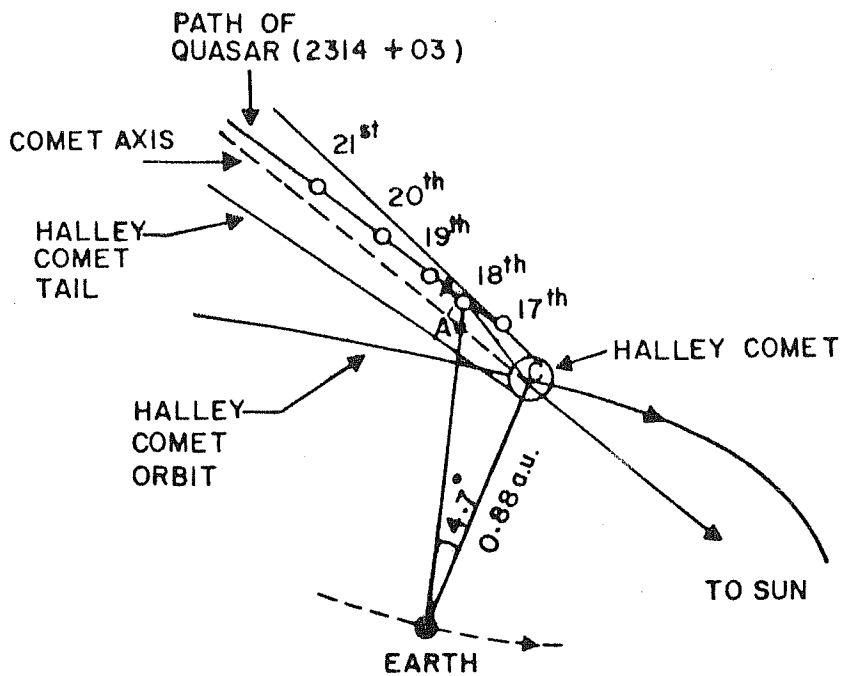


Fig. 4.2 Sketch of geometry of occultation of PKS 2314+03 by Halley's Comet.

shows some basic parameters regarding this geometry. On 18 December 1985, the angle comet-Earth and source was 4.7° and the comet's position angle was about 66° . The source 3C 459 was 87.5° away from the Sun. Starting from 2 December, only background scintillations (~ 2 Jy) were observed as the angle source-Earth-Sun was about 90° . On 18 December, an appreciable increase in the scintillations of 3C 459 were recorded when the distance from the comet nucleus to the point of intersection of the line of sight (Earth and source line) with the tail (AC in Fig. 4.2) was 0.12 AU. This increase in scintillations was about 6 times the background scintillations and about 1.5 times the average maximum scintillations recorded for this source at 103 MHz due to solar plasma around 30° elongation.

Fig. 4.2 is a copy of the recordings made during the occultation. Originally, there are three outputs from the correlation type receiver namely, COS, SIN and Scintillometer which are recorded on a strip chart as well as on a digital magnetic tape (Chapter 3). As there were no scintillations on the COS channel, the latter is not shown in this figure. As is evident from this figure, the scintillometer and SIN channels show the maximum scintillations on the 18th. These scintillations progressively reduced from 19th to 21st. In Fig. 4.3, the top trace in each panel shows the SIN output, while the bottom trace shows the scintillometer output. The chart speed on 17 and 18 Decem-

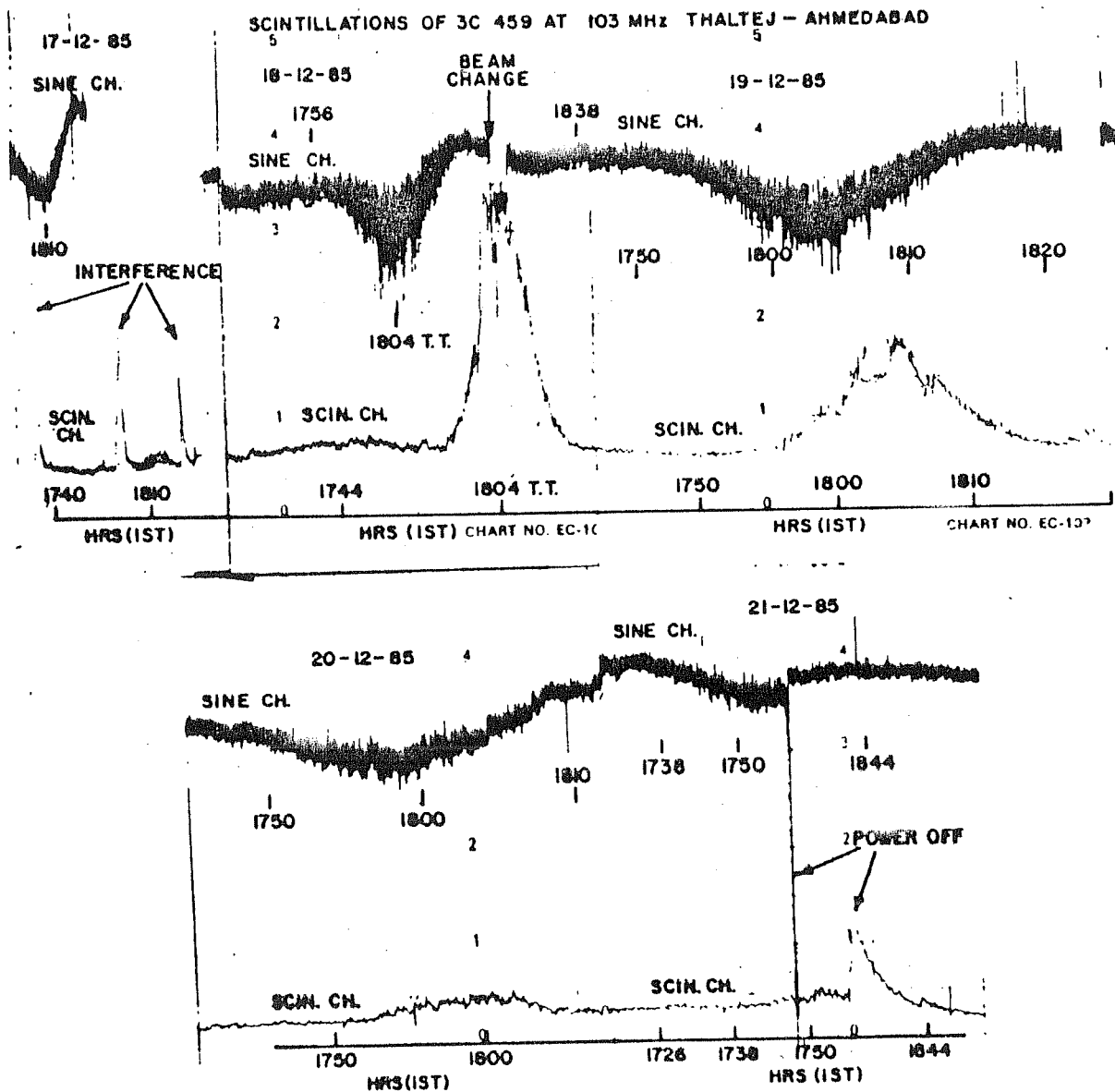


Fig. 4.3 103 MHz recordings during the occultation. Scintillometer and SIN channels show maximum scintillations on 18 December. These scintillations progressively reduced from 19 to 21 December. The top trace in each panel shows SIN output while bottom trace shows scintillometer output. Chart speed on 17 and 18 Dec. was 5 and 10 cm/hr. and 20 cm/hr. thereafter.

ber was 5 and 10 cm/hr respectively, and 20 cm/hr thereafter.

4.3 Data Analysis and Results

The IPS data were recorded on a magnetic tape as well as on a strip chart (as described in chapter 3). From these data the following information was derived:

4.3(a) Scintillation Spectra

Fig.4.4 shows scintillation spectra of the source, computed for 17 through 20 December. It is clear that the area under the curve, which is proportional to the scintillating power, is maximum for the 18 December. Solid lines are least-squared fits to data points. Error bars are standard error. Broadening of the spectra should be noted for 18-20 December. The spectral indices of the simple power-law fits to the high frequency (above 0.6 Hz) data are 2.83 ± 0.20 , 2.26 ± 0.15 , 2.31 ± 0.14 and 2.40 ± 0.17 or the average power-law index works out to be 2.45 ± 0.25 . This corresponds to a wavenumber spectral index of about 3.45, which is close to that expected for a three-dimensional Kolmogorov density spectrum. An average scintillation periodicity estimated from the auto-correlation analysis of the spectra turns out to be about 1 sec.

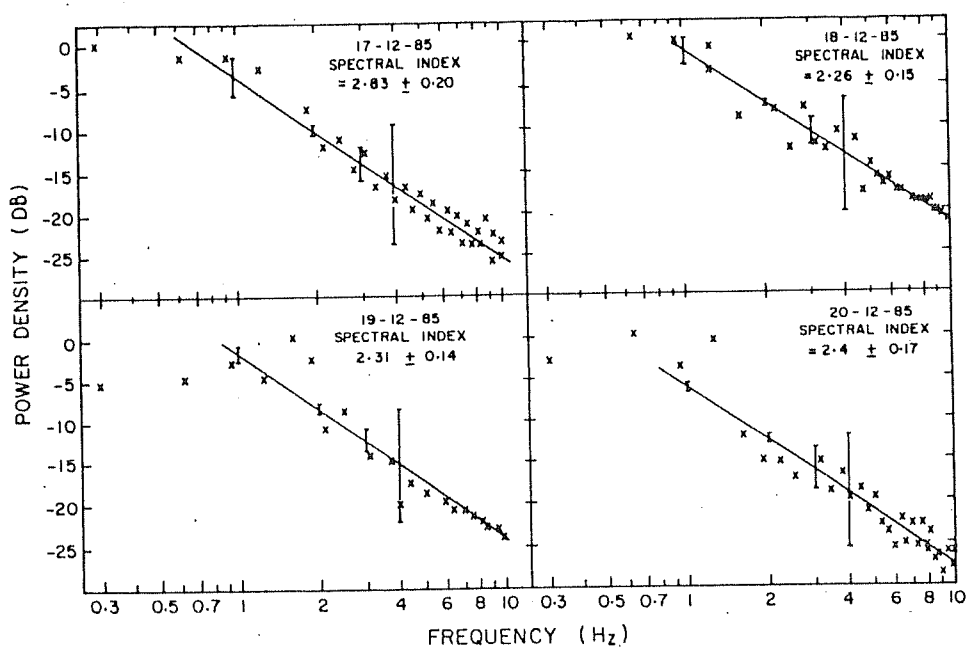


Fig. 4.4 Scintillation spectra of PKS 2314+03 on 17 through 20 December 1985. Solid lines are least-squared fits to data points. Error bars are standard errors. Note broadened spectra on 18, 19 & 20 December.

4.3(b) Calculation of Scintillation Index

An important parameter, scintillation index (m) is defined as

$$m = \frac{\Delta S}{\bar{S}} \quad \dots (4.a)$$

where ΔS is the r.m.s. scintillating flux and \bar{S} is the average flux of the source. ΔS and \bar{S} were calculated using scintillometer output and system calibrations (described in chapter 3). We obtained $\bar{S} = 43$ Jy and the ΔS values were calculated to be 10.75, 6.45, 3.01 and 2.15 Jy on 18 through 21 December 1985 respectively (Appendix I). The corresponding scintillation indices were 0.25, 0.15, 0.07 and 0.05 respectively.

4.3(c) Calculation of Scale-Size of Irregularity in the Ion-Tail

Assuming the velocity, v of the plasma density irregularities of 100 Km/s (upper limit), (Ershkovich, 1980), the scale-size was calculated to be 100 Kms. by using

$$a = v \times t \quad \dots (4.b)$$

where 'a' is the irregularity scale-size

't' ~ 1 sec., average periodicity of the scintillations.

4.3(d) Calculation of r.m.s. deviation, ΔN , of plasma density

For radio waves from a compact source, incident coherently on a plasma slab (the plasma tail of the comet P/Halley) of thickness 'L', the r.m.s. phase deviation along the line of sight to the source is expressed as (Cohen et al. 1967)

$$\phi_0 = 2^{\frac{1}{4}} \cdot \pi^{\frac{1}{4}} \cdot r_e \cdot \lambda \cdot (a \cdot L)^{\frac{1}{2}} \cdot \langle \Delta N \rangle \quad \dots (4.c)$$

where r_e = Classical electron radius,

λ = Operating wavelength, and

$\langle \Delta N \rangle$ = average r.m.s. change in plasma density

Eqn. (4.c) is true for a gaussian electron density correlation function. Under weak scattering condition ($\phi_0 \ll 1$ radian) Mercier (1962), eqn. (4.c) can be rewritten as

$$m = \frac{3}{2} \cdot \pi^{\frac{1}{4}} \cdot r_e \cdot \lambda \cdot (a \cdot L)^{\frac{1}{2}} \cdot \langle \Delta N \rangle \quad \dots (4.d)$$

With the help of eqns. 4(a-d), ΔN can be calculated. The value of 'L', the projected width

of the ion-tail used was 5×10^5 Km (from the image taken on 10 March 1986 by using the UK Schmidt telescope in Australia). The values of ΔN calculated were 1.82, 1.08, 0.36 and 0.35/c.c. on 18 through 21 December respectively.

$\therefore \Delta N$ on 18 December $\sim 2 \pm 0.25$ /c.c.

4.3(e) Electron Density, N in the Plasma Tail

The estimation of plasma density 'N' in the cometary ion-tail was made assuming ΔN proportional to 'N' in the tail. These values of ΔN and N in the case of solar plasma are known at any heliocentric distance by using (radial distance)⁻² dependence for both of them. Now, at a particular distance from the Sun, ΔN in the cometary tail was obtained from the present observations, while the same for the solar wind outside the tail was estimated using (distance)⁻² dependence. Also, the values of $(N)_{\text{solar}}$ are known for that distance. Hence, by comparison $(N)_{\text{cometary}}$ was calculated for that distance. This procedure is elaborated below for 18 December 1985.

On 18 December the ΔN value in the plasma tail was calculated from observations at anti-sunward radial distance, 1.34 AU from the sun which is

about 2/c.c. Now, ΔN and N in the case of solar plasma (calculated) at 1.34 AU (outside the tail), (Rees et al. Private communication) are .06 and 6/c.c. At this distance the ratio

$$\frac{(\Delta N)_{\text{comet}}}{(\Delta N)_{\text{solar}}} = \frac{1.82}{.06} = 30.34 \quad \dots(4.e)$$

the same ratio of N_{comet} and N_{solar} is assumed to hold good at 1.34 AU from the sun.

$$\text{i.e. } \frac{(N)_{\text{comet}}}{(N)_{\text{solar}}} = 30.34 \quad \dots(4.f)$$

or

$$N_{\text{comet}} = 182/\text{c.c.} \quad \dots(4.g)$$

$\therefore N_{\text{comet}} \approx 200 \pm 25/\text{c.c.}$ at 0.12 AU from cometary nucleus.

In-situ measurements made by the American spacecraft ICE, in March 1986 gave the range of N in the ion-tail of comet Halley, 20 - 600/c.c. The value of N estimated from the present IPS observations falls within this range.

- 4.3(f) The value of ΔN in the ion-tail; calculated from the Kolmogorov spectrum

The value of $\Delta N = 1.82/\text{c.c.}$ on 18 December 1985, was calculated assuming a gaussian irregularity spectrum. However, a Kolmogorov spectrum for turbulent media such as the solar wind, Earth's atmosphere and the stellar wind is more realistic. An attempt has been made to estimate the value of ΔN by assuming a Kolmogorov turbulent plasma in the ion-tail of comet Halley. Lee and Jokipii, (1975a) have shown that the correlation function of phase also has a Kolmogorov spectrum

$$P_{\phi}(q) = A(1 + q^2 L^2)^{-\alpha/2} \exp(-q^2 l^2/2) \text{ for } L \gg l$$

...(4.h)

where L = Coherence or outer scale

l = inner scale

q = wavenumber

This spectrum is

flat for $q < L^{-1}$

power-law with index $-\alpha$ for $L^{-1} < q < l^{-1}$

and cut off for $q > l^{-1}$.

Usually $-4 < \alpha < -3$ and particularly $\alpha = -11/3$ for

Kolmogorov spectrum. A , a constant is defined as

$$(\alpha/2 - 1) L^2/\pi; \quad \text{for } L \gg 1 \quad \dots(4.i)$$

Lee (1976), has shown that the correlation scale of intensity is

$$l_c = 1, \quad \text{for } l > (Z/K)^{\frac{1}{2}}$$

$$= (Z/K)^{\frac{1}{2}} \quad \text{for } l < (Z/K)^{\frac{1}{2}}$$

where Z is the distance to the observer and $K = 2\pi/\lambda$.

$l_c = v \cdot t_I = 100$ Km; since $v = 100$ Km/s (assumed) and t_I (periodicity of intensity variation) estimated to be about 1 sec. So, in the present case, $l_c \neq (Z/K)^{\frac{1}{2}}$, therefore we assume $l_c = 1$, inner scale of turbulence in the plasma tail of the comet, which is about 10^2 Km. Assuming the outer coherence scale, L , to be comparable to the width of the cometary tail, $L \sim 5 \times 10^5$ Km and taking the value of the scintillation index on 18 December 1985, which is about 0.25, we get $\Delta N = 1.4/c.c.$ for a Kolmogorov turbulence. This estimation is worked out as follows

$$\phi_o^2 = \frac{M_z^2}{A(\frac{z}{K})^2 \cdot 8\pi \cdot \Gamma_{7/6} \cdot l^{-7/3} \cdot L^{-11/3}} \quad \dots(4.j)$$

where M_z is scintillation index.

This equation gives the value of ϕ_o^2 to be about $\approx 3.6 \times 10^3$ radian².

Now, writing ΔN^2 as (Lee and Jokipii, 1975b)

$$(\Delta N)^2 = \frac{\phi_o^2}{76.8 \pi^{7/2} \cdot L \cdot r_e^2 \cdot K^{-2} \cdot D \cdot \frac{\Gamma_{11/6}}{\Gamma_{1/3}}} \quad \dots(4.k)$$

and taking $L = D$, this equation gives the value of ΔN to be about 1.4/c.c. for a Kolmogorov turbulence in the ion-tail.

It is very interesting to note that this value of ΔN , 1.4/c.c., is very close to the value of 1.82/c.c. calculated assuming gaussian turbulence in the cometary ion-tail. Also, the average wavenumber spectral index turns out to be very close to the Kolmogorov value ($-11/3$).

These parameters alongwith other calculated/estimated parameters are shown in Table 4-II.

4.4 Discussion

The present IPS observations were made when the solar elongation of the source 3C 459 was $\sim 90^\circ$. At such solar elongations the scintillation recorded, if any, are weak, as the telescope points far away from the Sun where the solar plasma and irregularities are sparse. Any possibility of interference causing such scintillations is ruled out because the scintillations recorded were maximum on 18 December and then progressively decreased on 19 and 20 December. No correlation was observed between the enhancement and ionospheric phenomena such as sporadic E and spread-F. Solar activity during the period of these IPS observations was 'very low', while geomagnetic activity was 'quiet to unsettled' with no Sc-type magnetic storms as reported by (Pre. Report and Forecast of Solar Geophysical Data Joint NOAA-USAF Space Environment Service Center, 1985). During this period, IPS observations of five other scintillating and non-scintillating sources were made, some of which were within 8° declination of the occulted source. None of these sources, except the quasar PKS2314+03(3C 459) showed any enhancement of scintillations. Hewish et al. (1985) showed that interplanetary transients cover a solid angle of helio longitude and latitude of $\sim \pi/2$ Sr. Also, according to them, there is a strong correlation between enhancement in scintillation and mean plasma density along the line of

sight to a source. As the enhancements in scintillations were recorded only in the case of 3C 459, the density increase was restricted in that direction only. We, therefore, concluded that the observed enhanced scintillations of 3C 459 were caused by the ion-tail of the comet Halley.

There are a few other observations of occultation of radio sources by cometary ion-tails. These will now be discussed and compared with our IPS observations at 103 MHz made during the pre-perihelion period.

Ananthakrishnan et al. (1975), reported fluctuations in the intensity of the extragalactic source PKS 2025-15 observed during its occultation by the coma and tail of the comet Kohoutek (1973f) on 5 January 1974. These observations were made at 327 MHz using the Ooty radio telescope. At the time of these observations the solar elongation of the source was 20° . These authors concluded that no radio emission above the confusion limit of the Ooty radio telescope could be detected from the comet Kohoutek (1973f). But fluctuations in the intensity of the occulted source were observed. (Although the authors did not uniquely attribute these fluctuations to the plasma in the ion-tail). However, Lee (1976) interpreted these scintillations as caused by the turbulent plasma in the ion-tail of the comet even though their periodicity was about 10 sec.

Slee et al. (1987) reported enhancement of scin-

tillations when the compact radio source 1827-360 was occulted by the Halley's comet on 29 March 1986 (Post-perihelion period). This was as much as 4 times the background scintillation level. These observations were made using Parkes 64-m telescope at 408 MHz. During these observations, the solar elongation of the occulted source was 89° and the geocentric velocity of the comet Halley was $\sim 40 \text{ Kms}^{-1}$. The topocentric and heliocentric distances of this comet were 0.576 and 1.143 AU respectively and the projected distance from the nucleus, at which the tail passed in front of the source, was $5.4 \times 10^6 \text{ Km}$. These authors have deduced ΔN in the ion-tail to be 1.8/c.c. for a gaussian electron density correlation function. The same for a Kolmogorov power-law spectrum, with an inner scale of 100 Km and an outer scale of $4.8 \times 10^5 \text{ Km}$, was estimated to be 1.4/c.c., which is very close to the value for a gaussian spectrum. These results agree well with the results described earlier.

Hajivassiliou and Duffett-Smith (1987), used the data recorded at Cambridge during the IPS survey at 81.5 MHz to make a retrospective search for enhanced scintillation caused by cometary tails. The data covered the period May 1978-March 1981 and comprised daily measurements of the r.m.s. scintillating flux density on about 2000 radio sources at all values of right ascension north of declination -10° . From these data base, these authors

found a sample of 35 comets out of which, 12 comets were identified as sufficiently bright to promise an effect and whose tails occulted about 45 bright scintillating sources observed in the survey. They concluded that there was no convincing evidence for enhanced scintillations of radio sources due to plasma density irregularities in the ion tails of the comets.

The observations of Hajivassiliou and Duffett-Smith were not really planned for occultation events by cometary ion-tails. The visual magnitudes of 8 out of 12 comets were in excess of 10 and had no reports on tail lengths of 6 comets; the remaining 5 comets had tail lengths of less than 2° and only one comet had a tail length of 5° . Their telescope could observe each source only for 2 minutes. Therefore, there were 58% chances of missing an occultation. In addition, comets slow proper motion which implied large uncertainties in the calculated moments of the occultations which confused their data. These authors therefore concluded that their observations did not entirely rule out the possibility of scintillations caused by cometary tails, since the comets used by them were faint and many of them carried no report of a tail being observed.

Ananthakrishnan et al. (1987) attempted to observe scintillations of four radio sources occulted by the ion-tail of the comet Halley at 327 MHz, using the Ooty radio

telescope. These sources were: 2052-106 ($\Delta S \approx 0.5$ Jy), 2021-168 ($\Delta S \approx 0.3$ Jy), 1921-293 ($\Delta S \approx 5$ Jy) and 1817-391 ($\Delta S \approx 1.2$ Jy). The last source was confused with 1815-391. Each occulted source, together with the corresponding nearby control sources, was observed for 15-20 min. alternated between 10 min. of observations of each of the control sources. Each observation was made for three days, the middle one being the day of occultation spread over 6-9 hr.

A description of only three occulted sources is given by these authors. The source 2052-106 was observed during 10-12 February; source 1817-391 was observed on 1 and 3 April and the source 1921-293 was observed during 23-25 March 1986. Based on these observations, the authors concluded that no significant increase in the level of turbulence was observed that could be attributed to the plasma tail.

These observations were not made in favourable conditions which are governed mainly by proper solar elongation of the source and the conditions of the cometary plasma tail. The solar elongation of the source 2052-106 during the observations was approximately 10° . Fig. 4.5 shows the geometry of the occultations of PKS 2314+03 and 2052-106 by Halley's plasma tail during 18-20 December 1985 and 11 February 1986. At 327 MHz the maximum scintillation of a scintillating source due to solar plasma occurs around

14° solar elongation. Consequently, bulk of the scattering took place in a relatively thin layer of the solar plasma centered around the point of closest approach to the source 2052-106. Corresponding control sources were also within 12° of the Sun. Therefore, the enhancement due to the cometary tail was not detected. The source also got broadened due to the strong scattering, resulting in reduction of the scintillations. Furthermore, due to the nearly 18° inclination angle between the ecliptic and the orbital plane of the Halley's comet, this line of sight might intersect the cometary tail at a point much towards its far end; and it will not intersect at all if the two planes were coincident. But this effect is only 5%. Thus, the event reported by Ananthakrishnan et al. was unsuitable to observe any enhancement of scintillations that would have been caused by a strong comet like Halley. The third occulted source was 2021-168 when the observations were made on 2 March 1986. Due to poor signal-to-noise ratio no observations are reported in their paper. This is very likely due to a disconnection event (DE) on 1 March UT which might have made the occultation ineffective. In the case of DE's, the entire plasma tail uproots itself from the head of the comet in the anti-sunward direction and after about a couple of days, it is replaced by new plasma tail. If such observations are made during DE's, scintillation may not be caused. The observation of the

third occulted source, 1921-293 is shown to be made on 24 March 1986. An enhancement of $\sim 10\%$ was shown by this source when it was within 10 arcmin. of the ion-tail. The last occulted source in their investigation was 1817-391 with its control source 1827-360. This observation was made on 1 and 3 April. From their Fig. 3(a), it can be estimated that the enhancement in the case of the occulted source was about 60%, while that for the control source (1827-360) was about 20%. Even then they described these two enhancements as similar. The DE's were reported by IHW participants and prepared by Dr. Niedner, Jr. NASA/GSFC (Private Communication).

Important information, regarding these observations, is summarised in Table 4-III.

4.5 Conclusions

As has been described earlier, a few attempts were made to record enhanced scintillations of compact radio sources attributable to density irregularities in the occulting cometary plasma tails. In addition, Hajivassiliou and Duffett-Smith (1987) analysed an extensive data base of IPS of about 2,000 sources recorded during 1978-81. They came across many events of occultations of scintillating sources by several comets. Most of these comets were faint and there was no information on their cometary tails. Also, due to their very short time (2 minutes) of observations on each source, nearly 58% of the occultation events

were missed. Due to these uncertainties of observations they concluded that they could not entirely rule out the possibility of cometary plasma tails giving rise to enhanced scintillations of radio sources.

The recent observations of Ananthakrishnan et al. (1987) studied in reality three events of occultations of radio sources by the Halley's plasma tail. We have indicated that one of the events reported by these authors failed to observe enhanced scintillations attributable to the cometary tail due to very unfavourable geometry during that event. During another event the Halley's tail was very likely affected by a DE. In the case of the events during 1-3 April 1986, their observations do indicate enhanced scintillations. On 1 April, there was substantial enhancement in the scintillations and on 24 March, this enhancement was $\sim 10\%$. In both these cases the ion-tail was within 10 arcmin. of the line of sight. These were misinterpreted in terms of reasons other than the cometary plasma tail.

The important requirements of favourable geometry of occultation, monitoring of background level of scintillations during and after an occultation event, covering of a sufficiently large region around the occulted source to monitor effects of interplanetary transients, geomagnetic storms and ionospheric phenomena and complete information on the cometary plasma tail were satisfied during our

observations at 103 MHz in December 1985. We, therefore, concluded that the enhanced scintillations observed by us were caused by the Halley's plasma tail.

In view of the importance of studying the plasma tail by radio occultation method, it would be beneficial to make coordinated observations at various wavelengths as described in chapter 7.

TABLE 4-I

Parameters* of Halley's comet

Date Dec. 1985	Solar elong- ation (Comet- Earth-Sun angle) in degree	Δ (Geocentric distance of comet) in AU	R (Heliocen- tric distance of comet) in AU	$\dot{\Delta}$ (Geocentric velocity of comet) Km/sec	\dot{R} (Heliocentric velocity of comet) Km/sec	Halley comet's declination (1950)
17	84.1	0.86	1.24	33.47	-26.74	+2° 36'.02
18	81.8	0.88	1.22	33.92	-26.76	+2° 7'.67
19	79.6	0.90	1.21	34.29	-26.78	+1° 40'.73
20	77.5	0.92	1.19	34.58	-26.79	+1° 15'.13
21	75.4	0.94	1.18	34.80	-26.80	+0° 50'.80

* IHW newsletter no.7.

TABLE 4-II

Calculated parameters from the occultation observations

Date (Dec. 1985)	Scinti- llating flux, ΔS (Jy)	Scinti- llation index, m	r.m.s. change in den- sity(ΔN) el/c.c.	Tailward distance from the nucleus to the line of sight in AU	Estimated density N el/c.c.
17	2.15*	0.05*	0.36*	0.080	36*
18	10.75	0.25	1.82	0.121	182
19	6.45	0.15	1.08	0.144	108
20	3.01	0.07	0.36	0.178	36
21	2.15*	0.05*	0.36*	0.204	36*

* Values equivalent to the control, (average) days.

TABLE 4-III

Summary of the recent cometary occultation events discussed in this chapter

Place & Frequency of operation	Observation period	Scintillating sources occulted	S Jy & solar elong.	Comet used	Information on cometary tail	Remarks
Ahmedabad (India) 103 MHz	18-20 Dec. 1985	PKS 2314+03 (3C 459)	11 Jy 85°	Halley	Length 10° No DE	3 days' observations Enhancement of scint. by factor of 6 over background scin.
Parkes (Australia) 408 MHz	29 Mar. 86	1827-360	10.6 Jy 89°	Halley	10° No DE	Enhancement of 4 times
Ooty (India) 327 MHz	11 Feb. 86	2052-106	0.5 Jy 10°	Halley	Nil	Solar wind contribution to scint. dominating
	2 Mar. 86	2021-168	0.3 Jy 37°	"	DE on Mar. 1 UT	S/N poor; no observations
	24 Mar. 86	1921-293	5 Jy 74°	"	Nil	-
	1 Apr. 86	1817-391	1.2 Jy 96°	"		Confused with 1815-391
Cambridge (UK) 81.5 MHz	May 1978 - March 1981	35	- 90°-100°	12 Comets	None for 6 comets; one comet 5°, rest less than 2°	58% chance of missing the occultation. No information on DE.

APPENDIX I

Calculation of scintillating flux (ΔS) and scintillation index (m) of 3C 459 during its occultation by the ion-tail of Comet Halley:

Scintillation index is defined as

$$m = \frac{\text{Scintillating flux, } \Delta S}{\text{Mean flux, } \bar{S}}$$

The mean flux of the source was calculated by using the system calibration, Fig. 3.6 and eqn. (3.a). This value was estimated to be about 43 Jy.

The scintillating flux, ΔS was estimated using eqn. (3.f) which is

$$\Delta S \approx 2 \sqrt{\Delta I} \text{ Jy}$$

where ΔI is the scintillometer deflection.

The value of ΔI , read from the strip chart (Fig. 4.3) of 18 December 1985, was about 27 and hence

$$\Delta S \approx 2 \sqrt{27} \approx 10.4 \text{ Jy}$$

$$m = \frac{\Delta S}{\bar{S}} = \frac{10.4}{43} \approx .242$$

This value of m , was used in further calculations of ΔN . Similar calculations were also made for the other dates of occultation.

CHAPTER FIVE

DISPLACEMENT OF INTENSITY PATTERN PRODUCED BY LARGE-SCALE DENSITY IRREGULARITIES

5.1 Introduction

Plasma density irregularities of different scale-sizes present in a turbulent medium cause refractive or diffractive scattering of incoming radio waves. If the size of the irregularity is less than or equal to the Fresnel distance, the scattering produced is diffractive otherwise, it is refractive. They are called 'small-scale' and 'large-scale' irregularities respectively. These small-scale irregularities cause various types of phenomena such as radio scintillations occurring in the Earth's ionosphere, IPM, ISM^{*}, etc. For example, in the case of IPS,

* Interstellar Medium

the typical size of the irregularities producing scintillations of the signal from radio galaxies are in the range of 10^2 - 10^3 Kms. Irregularities larger in sizes than this, are called large-scale irregularities. Such irregularities produce large phase-gradients across the wavefront of an incoming radio wave and shift the scintillation pattern itself without changing it. Due to this refraction, the apparent positions of radio sources undergo variations (Shishov, 1975). Propagation of waves in a turbulent medium has been discussed in detail by Chernov (1960) and Tatarski (1961).

Okoye and Hewish (1968) reported such an effect in the case of several strong radio sources. They attributed this effect to the scattering by large-scale (50-several hundred Kms) ionospheric density irregularities. They showed that the irregularities were essentially a day-time phenomenon and they exhibited seasonal variations with a maximum in winter. They estimated that ionospheric irregularities of scales of about 100 kms or more produced a phase deviation of about 40π radians corresponding to a refraction angle of about 8-10 arc minutes. Okoye and Hewish (1967) made observations of radio scattering in the outer solar corona and in the IPM using a 38 MHz interferometer with a baseline of 10 km. The variation of power-law index of scattering showed that the index decreased progressively at large distances in the range of

about 20-80 solar radii. They attributed this finding to the hypothesis that the instabilities grow progressively as the plasma is carried away from the Sun. Bougeret (1981) reported similar effect in the case of solar noise storm. He observed quasi-periodic fluctuations in the apparent positions of Type I solar radio sources and attributed these to electron density inhomogeneities associated with internal gravity waves in the F2-region of the ionosphere.

Shishov (1975) studied the possibility of measuring parameters of large-scale inhomogeneities in the interplanetary plasma by ground-based radio astronomical methods. His method was based on measuring the displacement of the scintillation pattern (caused by the refraction effect) of a radio source at two frequencies. An attempt was made by Cole and Slee (1980) during the IPS observations of the radio source 3C 273 on 10-11 October 1978 when its solar elongation was 13° , to find out the physical form of interplanetary irregularities producing the time variations of the intensity using a spectrum analyzer over a frequency range 280-520 MHz. Dynamic spectra of IPS of 3C 273, showed strong bands revealing increasing curvature towards lower frequencies. Typically, refraction angles of 0.22 and 0.77 arcsecs were observed at 520 and 280 MHz respectively.

Hewish (1980) explained the frequency drift observed by Cole and Slee (1980) to be similar to that observed in the scintillations produced by small-scale combined with the large-scale irregularities, the

IPS RECORDINGS OF 3C298 AT 103 MHz
THALTEJ, AHMEDABAD

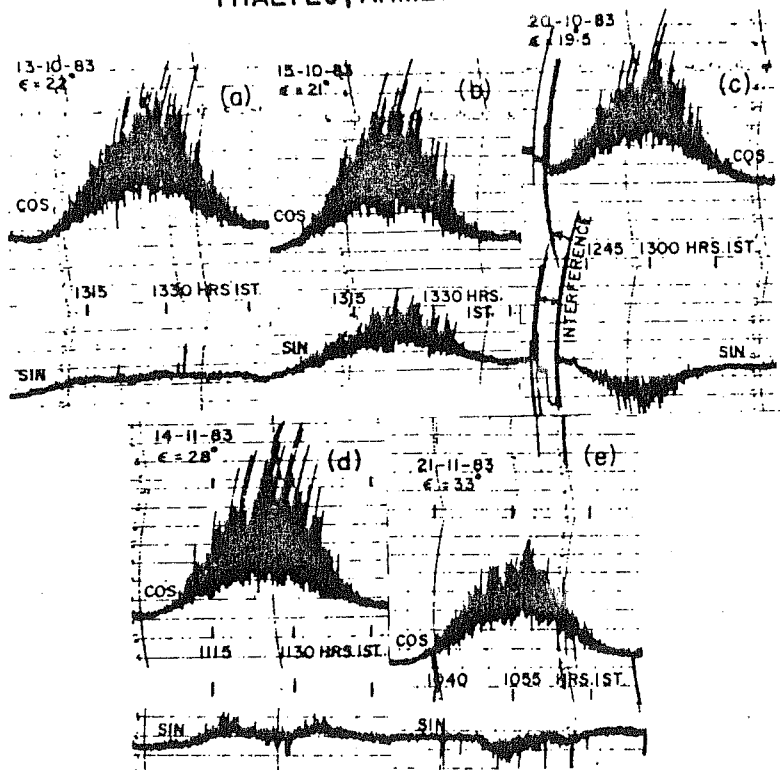


Fig. 5.1 Typical IPS records of 3C 298 showing (a) normal record and (b)-(e) records showing effects of large scale plasma density irregularities.

latter causing phase gradients across the wavefront. Hewish explained the frequency drift as caused by irregularities of scale size 4×10^3 Kms for a solar wind velocity of 400 Km/s. The estimated frequency drift was about ± 390 MHz/sec corresponding to a refraction angle of 0.2 arcsec.

Gapper and Hewish (1981) showed that the presence of refraction effects, produced by density irregularities in the solar wind, may be revealed by simultaneous measurements of intensity scintillation at two frequencies.

The observations reported here were made with a view to study the effect of large-scale plasma density irregularities in the ionosphere. The strong scintillating source 3C 298 was observed regularly for IPS studies using the R.T. at Thaltej at 103 MHz. During these observations, a quasi-sinusoidal scintillating wavy pattern was noted. An attempt is made to understand the nature of these irregularities causing such deviations.

5.2 Observations

The quasar 3C 298, angular size^{of} about 0.4 arcsec. at 81.5 MHz (Duffett-Smith 1976), was observed from 1982^{to} 1986. On an average, the typical elongation range covered each year was about 20° - 80° . Here, the description of the observations made in October-November 1983 is given. At the time of these observations the physical area of the

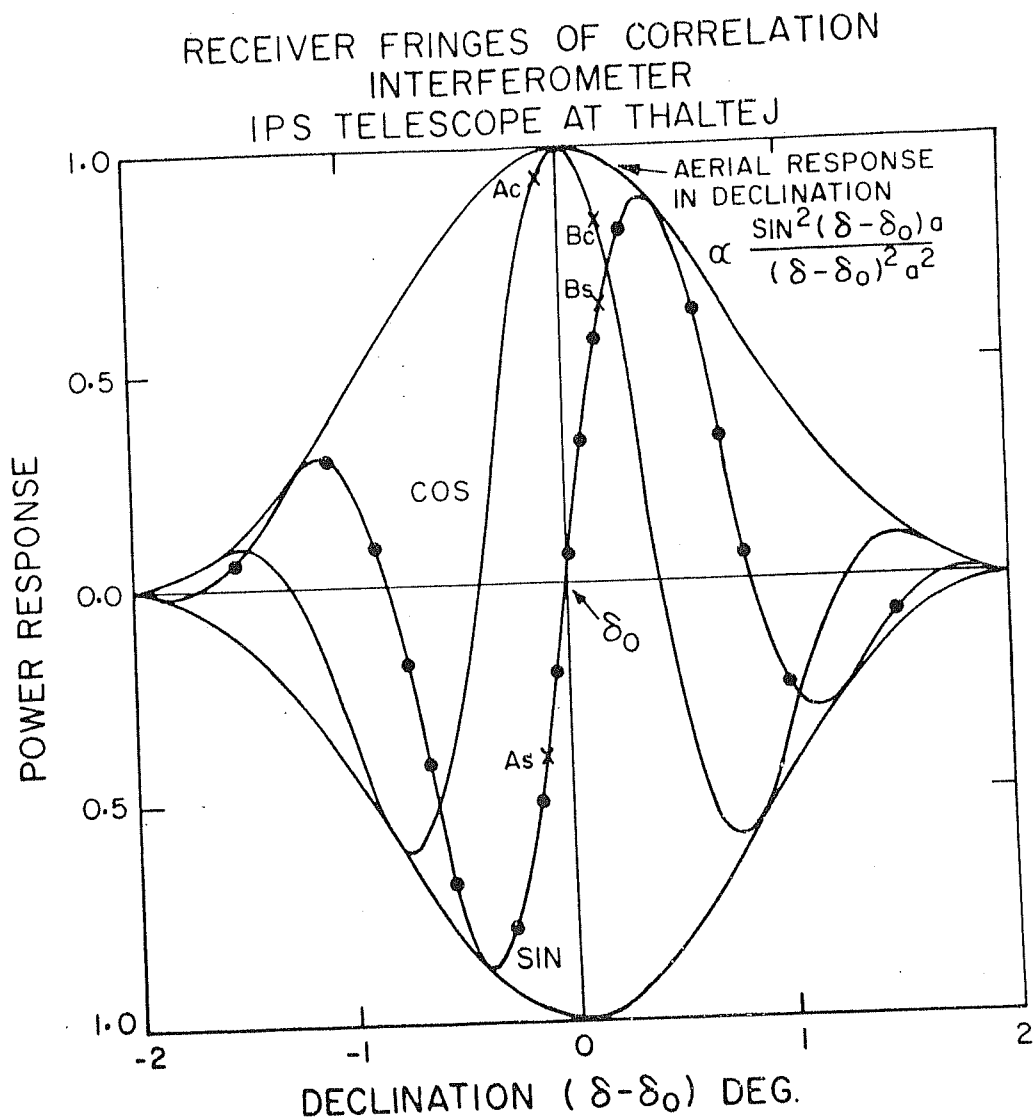


Fig. 5.2 Receiver fringes of correlation interferometer of radio telescope at Thaltej. A_c , B_c and A_s , B_s are assumed positions of 3C 298 on COS and SIN fringes.

R.T. at Thaltej was $5,000 \text{ m}^2$. The HPBW's of the antenna were 7.2° and 1.8° in R.A. and dec. respectively. Out of a total of 70 observations, 35 were in the elongation range 20° - 35° . These 35 observations can be grouped into five types and each of these types is shown in Fig.5.1.

During these observations (Fig.5.1,a-e), a wavy pattern was observed on the SIN channel on the strip chart (Fig.5.1d and e). Fig.5.1a represents the normal recording where the maximum scintillations and the dc flux of the source are seen on the COS channel; while on the SIN channel very small dc flux is seen.

Each event shown in Fig.5.1(a-e) can be explained with the help of Fig.5.2. This figure shows receiver fringes of correlation interferometer of the IPS telescope at Thaltej (Alurkar et al. 1985).

As mentioned earlier (in the chapter on the R.T. at Thaltej), the antenna array is divided into two halves, each comprising 32 rows of 32 dipoles each. The interferometer operation is effected by multiplying the response of the Southern half of the antenna aperture with its Northern half, the separation between their phase centers being 32 wavelengths or about 93 meters. The resulting antenna response in declination, together with the SIN and COS fringes of the correlation type receiver, are sketched

in (Fig.5.2). The half-power beam widths (HPBW_s) of this aerial response near zenith are about 1.8° in declination and 7.2° in right ascension. Such an interferometer in declination has an advantage that a radio source stays on the same SIN and/or COS fringes during its transit.

Fig.5.1(a), shows that the COS channel is having the maximum scintillating as well as the dc flux of the source, while the same is minimum on the SIN channel. The corresponding position of the source can be thought of as near the peak of the COS fringe (Fig.5.2) and near the zero crossing of the SIN fringe respectively. The recordings of Fig.5.1(b and c) on 15 October and 20 October show a good enhancement on the SIN channel also but in the latter case the deflection is in the reverse direction (comparing the direction on the COS channel). The record Fig.5.1(b) will result if the source positions were at B_C and B_S on the COS and SIN fringes in Fig.5.2 and the record (c) will result if they were at A_C and A_S .

The interesting events on 14 and 21 November are shown in Fig.5.1 (d,e) which correspond to solar elongations of 28° and 33° respectively. The wavy pattern on the SIN channel between 1118 and 1136 HRS is believed to be due to the change in apparent declination of 3C 298 from a position such as at B_S to very near zero-crossing and back to B_S within 18 min. of time. The event on November 21 also took a comparable time interval.

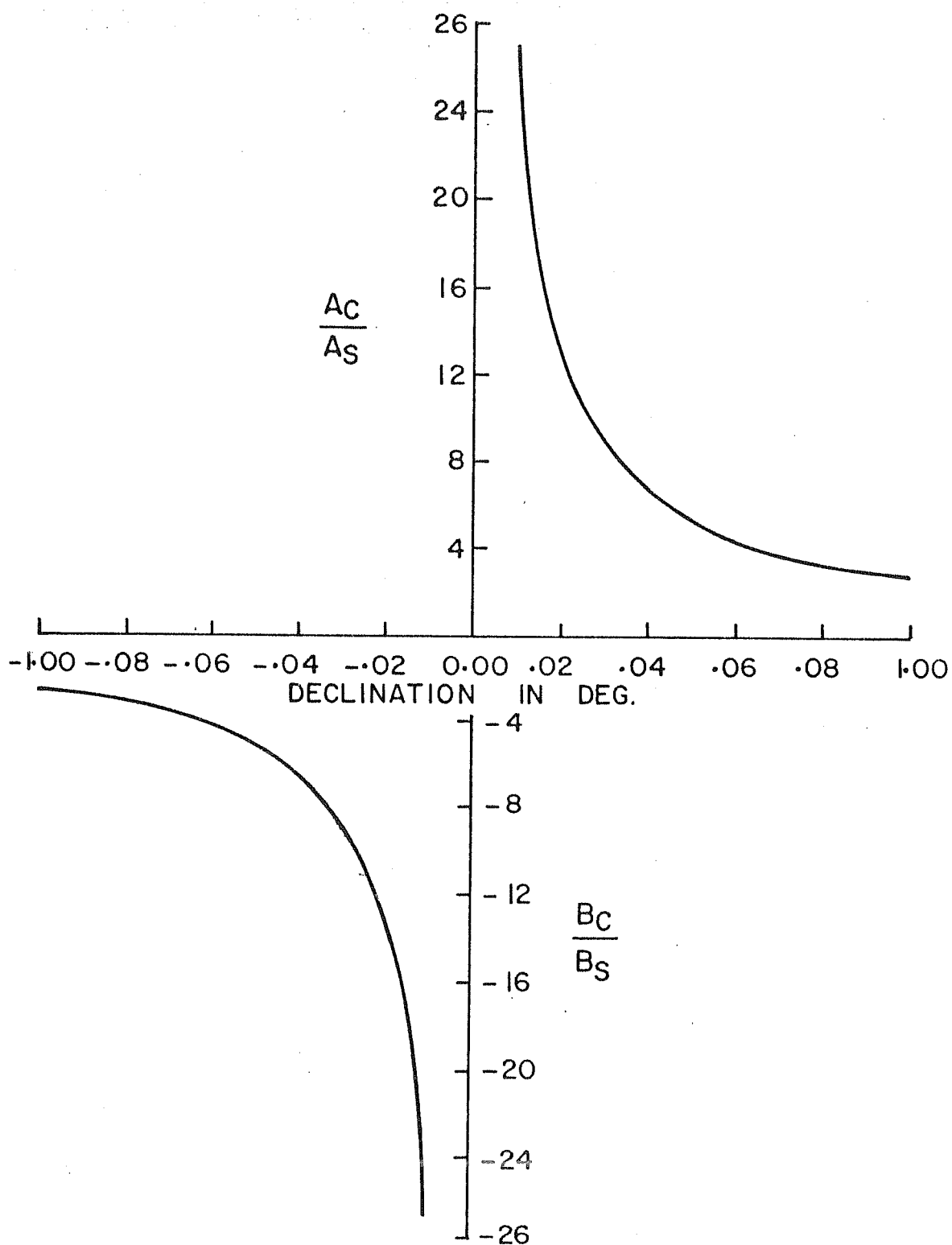


Fig. 5.3 A_C/A_S and B_C/B_S plotted against declination with the help of Fig. 5.2.

5.3 Analysis and Results

To calculate the change in declination of the source 3C 298 caused by the plasma irregularities from the variations in the mean flux level in the SIN channel, magnitude ratios B_c/B_s and A_c/A_s were plotted as a function of declination shown in Fig.5.3. This figure is plotted with the help of Fig.5.2, where the apparent position of the source is moved on the COS fringe and its ratio is taken with its position on the SIN fringe for the corresponding declination. Now, the observed ratios of average peak fluctuations of COS and SIN records in the presence of the events in Fig.5.1 (d,e) as well as during normal events were determined. For Fig.5.1 (d), this was done by extrapolating the peak flux on the SIN record between 1118 and 1136 HRS. The declination corresponding to these ratios were obtained from the graph of A_c/A_s and B_c/B_s as ^afunction of declination (Fig.5.3). The difference between these two values gave the maximum change in the declination of 3C 298. For the event on November 14, this amounted to about 5 arcminute in the declination plane.

Attempts are made to find out the density of plasma irregularities and their scale-size assuming that the irregularities were present in the ionosphere. Such irregularities could be due to gravity waves. Georges (1968) has classified them to be of the medium-scale. Taking

the value of ionospheric drift to be 100 m/sec (Sardesai et al. 1983), the scale-size 'L' of the gravity waves corresponding to the time interval of 18 min. in Fig. 5.1(d), turns out to be about 100 Km. Bougeret (1981) has also given the period and the horizontal wavelength of medium-scale gravity waves to be (12-40 min) and (50-300 Km) respectively.

At the latitude region in question, the ionospheric irregularities are not field-aligned; so the angular displacement in the direction of the drift would be the same as that in the declination plane which is 5 arcminute $\sim 1.5 \times 10^{-3}$ radian. The r.m.s. phase deviation, ϕ_o , caused by such irregularities can be calculated using the following formula (Alurkar et al. 1985)

$$\phi_o = \theta_r \cdot f \cdot L / c \quad \dots(5.a)$$

where θ_r is the angle of refraction,
 f is the operating frequency,
 c is the velocity of light.

On substitution of all these values in eqn. (5.a) the value of ϕ_o obtained is about 50 rad. This phase deviation, ϕ_o , is related to the integrated mean square deviation of ionization density $(\Delta N)^2 dz$, Booker (1981), as

$$\phi_o^2 = 4 r_e^2 \cdot \lambda^2 \cdot \sec \psi \cdot L \cdot \int (\Delta N)^2 dz \quad \dots(5.b)$$

where

r_e = classical electron radius, and

ψ = zenith angle of the source.

For normal incidence of the wave (i.e. $\psi = 0$) on the irregularities, this eqn. can be rewritten as

$$\phi_o^2 = 4.r_e^2 . \lambda^2 . L . \int (\overline{\Delta N})^2 dz \quad \dots (5.c)$$

This equation gives the value of $\int (\overline{\Delta N})^2 dz$ to be about $7.5 \times 10^{25}/m^5$. Assuming the thickness of the irregularity where the gravity wave exists to be equal to the thickness of the F-region (~ 300 Kms), the value of $\left[(\overline{\Delta N})^2 \right]^{\frac{1}{2}}$ turns out to be about 1.6×10^{10} el/m³, which is approximately 4% of the average ambient value of 5.8×10^{11} el/m³ Chandra et al. (1979), Titheridge (1972), Yeh and Liu (1974), Jain (1977), Vats and Deshpande (1980), Bougeret (1981) and Vats et al. (1981). Our estimation of some features of large-scale ionospheric irregularities is in reasonable agreement with that of these workers.

5.4 Discussion and Conclusion

The observations presented here were made during 1983-1986. The refraction was observed in day time in the months of October and November. Calculations of plasma density irregularities and their scale-sizes are in agreement with those of the previous workers. Our estimates

of irregularity scale-sizes (about 100 Km) and phase deviation (50 radians) caused by them are in good agreement with those reported by Okoye and Hewish (1968). Therefore, it is concluded that the refraction effect observed during IPS observations at 103 MHz was caused by large-scale density irregularities in the ionosphere.

Had the irregularities been in the IPM, the refraction caused at 103 MHz would have turned out to be about 6 arcsec. compared with the results at 280 and 520 MHz (Cole and Slee, 1980). This refraction angle is too small to be measured by the Thaltej correlation interferometer. Also, a wide band dynamic spectrum analyzer is required to observe the frequency drift effect produced by the large-scale interplanetary irregularities.

CHAPTER SIX

IPS OBSERVATIONS OF PSR 0531+21

6.1 Introduction

High resolution interferometry at 38 MHz (Hewish and Okoye, 1964) and lunar occultation observations at 26 MHz (Andrew et al. 1964) of the region of Crab Nebula showed the presence of a pulsed radio source (0531+21). Later, IPS observations (Hewish and Okoye, 1965; Bell and Hewish, 1967; and Antonova et al. 1971) showed the presence of a scintillating radio source, called 3C 144, at the same position as the pulsar (0531+21). Based on the observations of its angular size, pulse broadening, spectra and scintillation, Kenneth (1971) also concluded that the compact source is the pulsar NP 0532.

Armstrong et al. (1973), on the basis of 74 MHz observations, concluded that the scintillating flux of the compact continuum source was about 14% of that of the Crab Nebula. It had a gaussian shape of size of about 0.18 ± 0.01 arcsec. with the flux twice that of the extrapolated flux from the VLBI observations of the pulsed emission (Erickson et al, 1972 and Vandenberg et al. 1973). Armstrong and Coles (1978) pointed out that this discrepancy in the scintillating flux values (values estimated from IPS and VLBI observations) is due to the models used. Armstrong et al. (1973) estimated the flux by comparing the observed scintillation with the predictions of Readhead (1971). Scintillation index is defined observationally as

$$\frac{\text{r.m.s. flux}}{\text{Flux of the entire Nebula}} \quad (\text{Armstrong and Coles, 1978})$$

and in the Readhead's model as

$$\frac{\text{r.m.s. flux}}{\text{total compact source flux}}$$

Hence the estimation of the scintillating flux has been made with respect to the entire Nebula, which gives the larger value of the former (Armstrong and Coles, 1978). Readhead's model assumes the gaussian shaped solar wind turbulence. Power-law model for the same (Rumsey, 1975; Mariani, 1975) predicts a scintillation index about twice

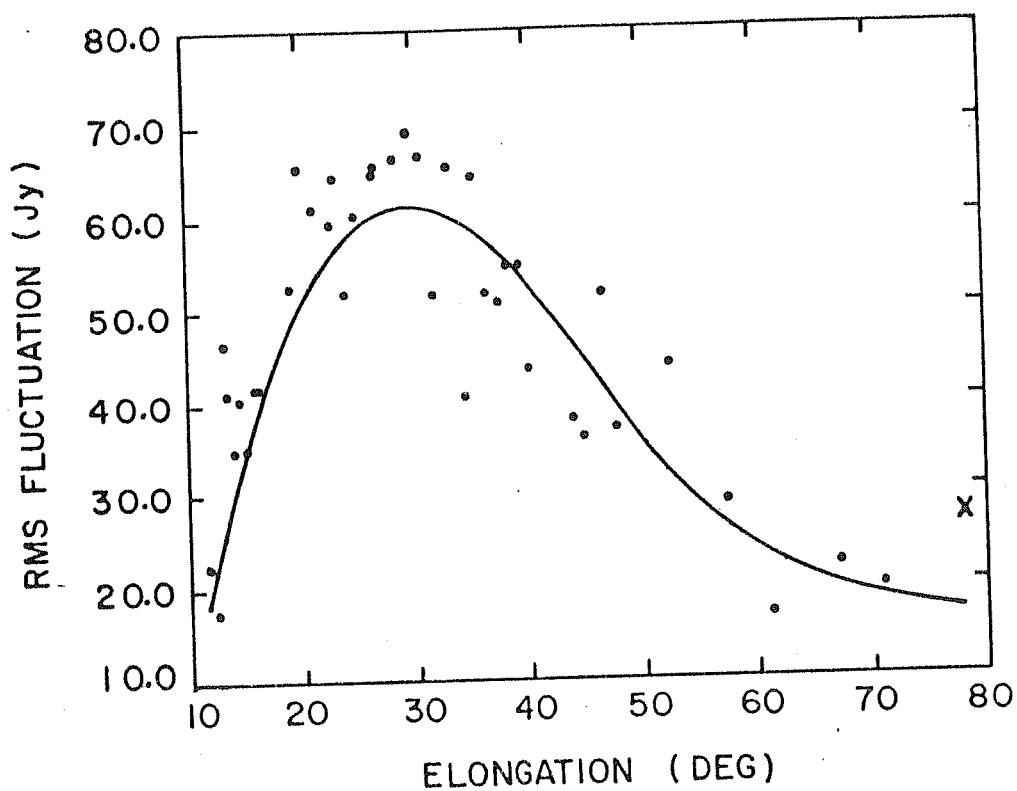


Fig. 6.1 R.M.S. fluctuation of the compact source flux plotted against its solar elongation. Solid line is a third degree polynomial fit to the data at 103 MHz.

the Readhead value for a given source. Hence this removes the previous disagreement with the VLBI estimated flux.

Therefore, it was interesting to make observations of IPS of 3C 144 over a wide range of elongation at 103 MHz in an attempt to find out whether or not these two sources (scintillating source 3C 144 and the pulsar (0531+21)) are identical. An estimation of its angular size and scintillating flux was made using gaussian and power-law models for the IPM.

6.2 Observations

The present IPS observations of 3C 144 were made regularly from May through September 1984 by using the Thaltej radio telescope. During these observations the antenna beam widths to half power at the local zenith were 1.8° and 3.6° in dec. and R.A. planes respectively. The solar elongation range covered during the observations, was about 10° - 80° . Analog as well as digital data recording systems were used. The data were corrected for undesirable noise and interference. Beyond about 70° solar elongation, the data points affected by ionospheric effects were excluded for the fitting of the polynomial to the IPS data.

6.3 Analysis and Results

Fig.6.1 shows the r.m.s. fluctuation of the scintillating flux of the compact source plotted against its

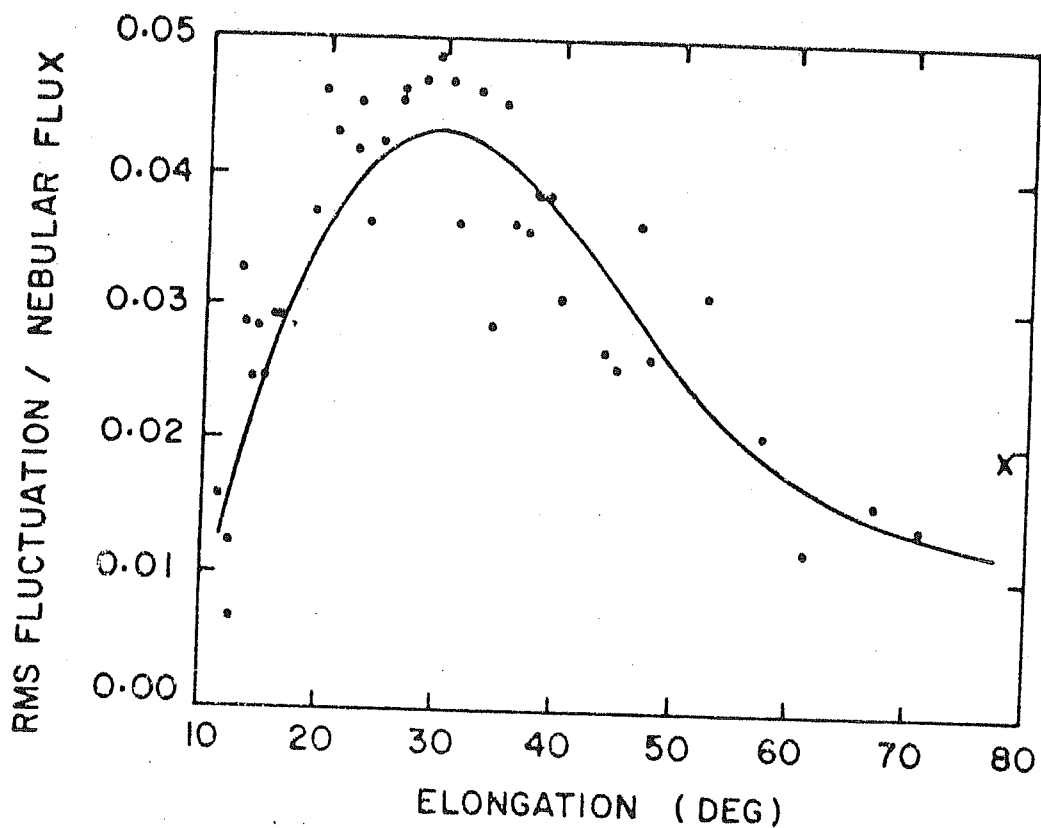


Fig. 6.2 R.M.S. fluctuation of compact source flux normalized by nebular flux plotted against its solar elongation. Solid line is third degree polynomial fit to the data at 103 MHz.

solar elongation. A polynomial of third degree is fitted to these data. The flux of the nebula was estimated to be 1623 Jy at 103 MHz from its value at 81.5 MHz (Readhead and Hewish, 1974) using the relation $S(f) \propto f^{-0.75}$ (where f is the operating frequency). Fig.6.2 shows the r.m.s. fluctuation of the scintillating flux of the source normalized by the flux of the nebula plotted against the solar elongation. A third degree polynomial is fitted to these data also. The uncertainties, on either side of the maximum r.m.s. fluctuations, could be 20%, while at the maximum it is about 10%. The maximum scintillation index occurs at about 30° solar elongation. Due to the well-known effect of broadening of the source due to strong scattering, there is a turnover in scintillation index for lower values of solar elongation. According to scintillation theory (Readhead, 1971), the r.m.s. flux at 30° depends on the flux of the scintillating component, its size and the shape of the density irregularity spectrum.

The scintillating flux values of the compact source for the gaussian and power-law models (Readhead, 1971; Rumsey, 1975; Mariani, 1975) turn out to be about 112 Jy and 95 Jy at 103 MHz respectively. These values have been calculated by assuming its size to be 0.2 arcsec. (Readhead and Hewish, 1974; Armstrong 1975). These values are about 7 and 6 percent of the Nebular flux. Fig.6.3 (Fig.3 of Armstrong et al. 1973) shows the scintillating flux values of the compact continuum source at various frequencies estimated from IPS observations (Bell and

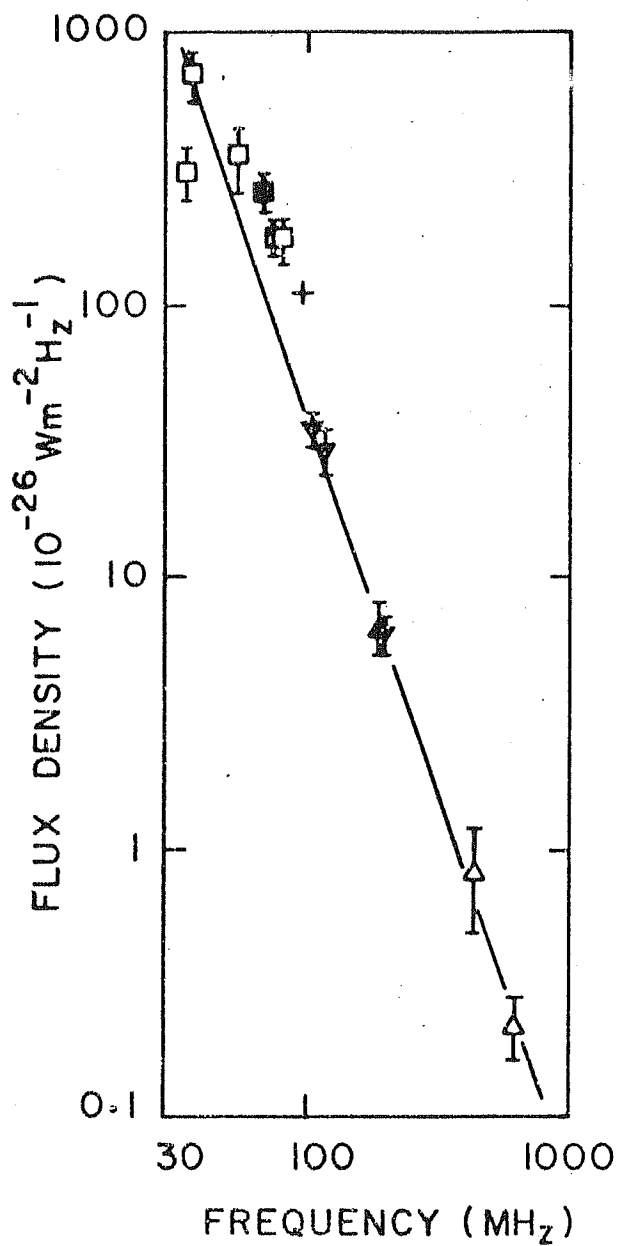


Fig. 6.3 Radio spectrum of compact source (Fig.3 of Armstrong et al. 1973). The line is a power law fit to the VLBI and pulsating flux measurements. Scintillating flux at 103 MHz from IPS observations is shown by +.

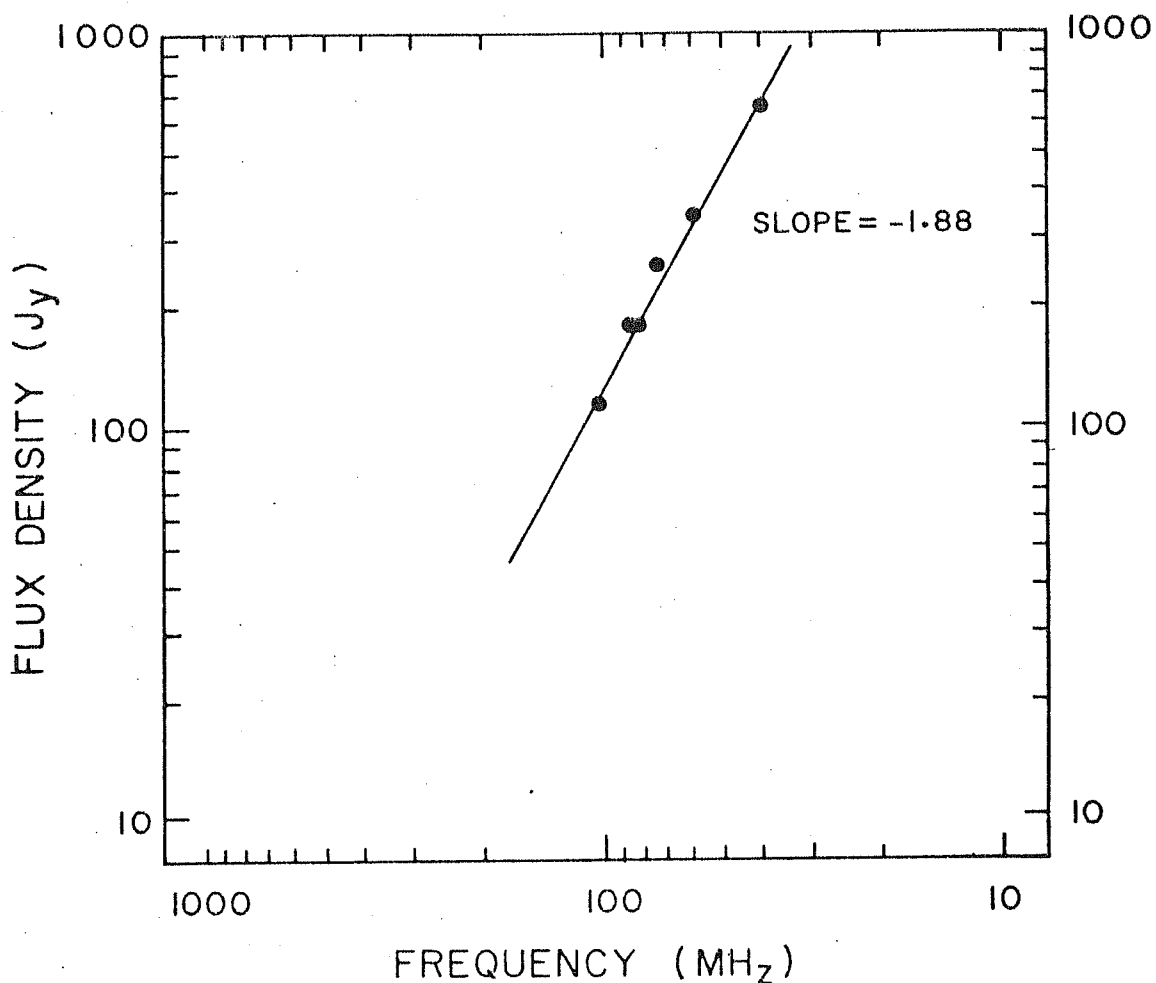


Fig. 6.4 Flux density as a function of frequency. Flux densities at frequencies 40-86 MHz are taken from Armstrong et al. (1973) and that at 103 MHz is from the present work. The plot has a slope of about -1.88, indication that $S(f) \propto f^{-1.88}$.

Hewish, 1967; Matveenko and Pynzar, 1969; Antonova et al. 1971 and Armstrong et al. 1973) together with those obtained using VLBI observations (Erickson et al. 1972 and Vandenberg et al. 1973) and pulsating flux measurements (Rankin et al. 1970).

The scintillating flux of the compact source at 103 MHz extrapolated from the pulsar flux values is about 48 Jy (Fig.6.3). Therefore our estimated scintillating flux values of the compact source (3C 144) for gaussian and power-law models are about 2.4 and 2 times this extrapolated flux. At 74 MHz the flux (256 Jy) of the compact source for a gaussian model is 14% of the Nebular flux (Armstrong et al. 1973). Fig.6.4 shows the flux values, S , at different frequencies (40-86 MHz) given by Armstrong et al. (1973) together with our value at 103 MHz, plotted against the operating frequencies. It has a slope of about -1.88 , indicating that $S(f) \propto f^{-1.88}$.

The data are fitted with the gaussian model for 0.2 arcsec. source, computed by using the method of Kemp (1976). This is shown in Fig.6.5 where the scintillating flux of the compact source at 103 MHz normalized by the compact source flux is plotted against solar elongation, ϵ . This fit is rather unsatisfactory for elongations less than about 15° . This may be due to contamination by the solar radiation closer to the Sun.

An attempt has also been made to fit to the present IPS data of 103 MHz, the power-law model (Rumsey, 1975).

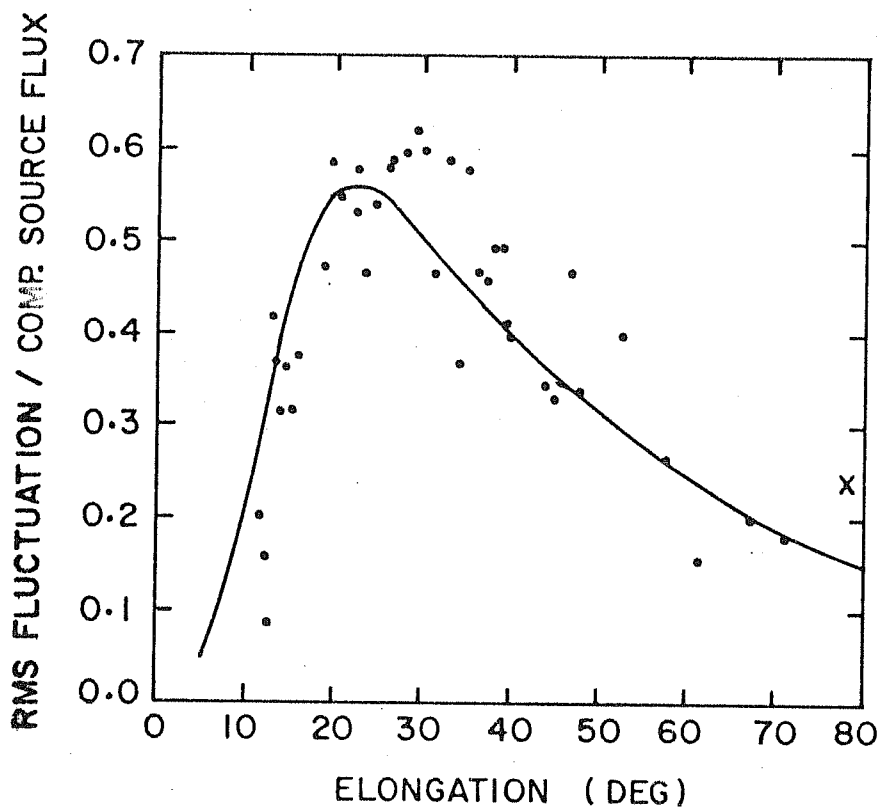


Fig. 6.5 R.M.S. fluctuation of the compact source flux at 103 MHz normalized by the compact source flux is plotted against its solar elongation. Continuous curve is for gaussian model of 0.2 arcsec source. The model computations were made using the method of Kemp. (1976).

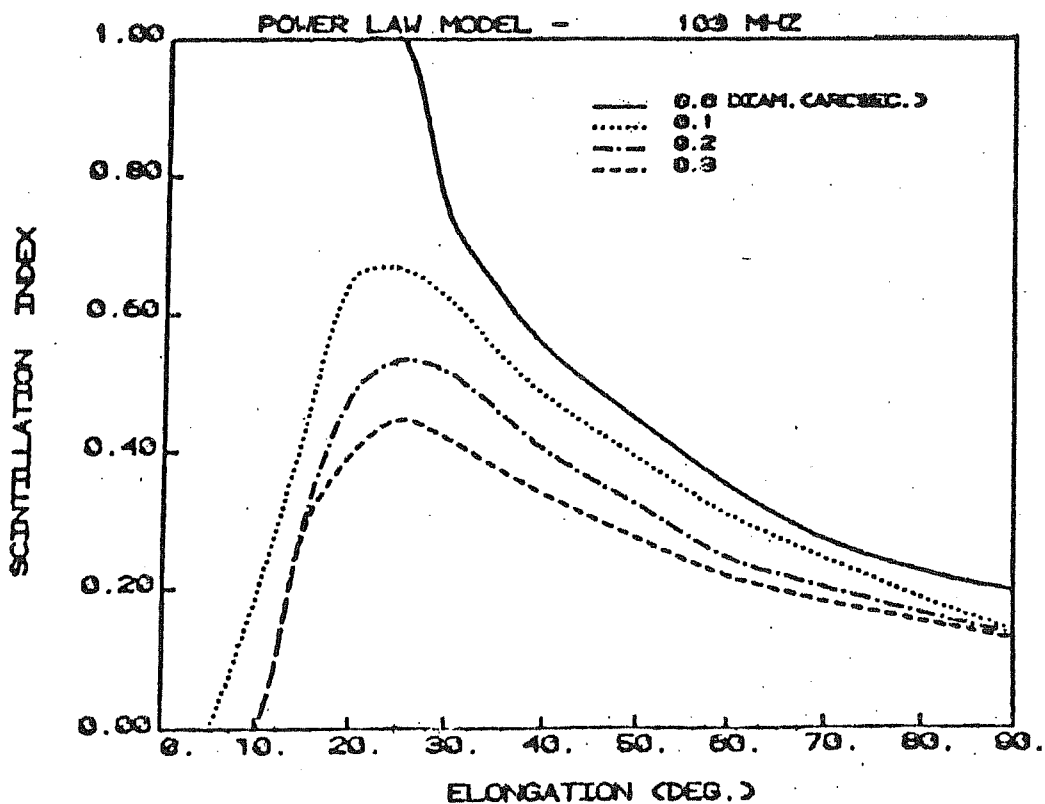


Fig. 6.6 Curves of scintillation index vs. solar elongation after scaling the computations of Marians (1975) to 103 MHz.

This model is appropriate for a thin plasma layer of strong scattering with a spatial wave-number spectrum for the refractive medium given by

$$P(q) \propto q^{-\alpha} \quad \dots(6.a)$$

where q is a 3-dimensional spatial wave-number.

Taking $\alpha = 3$,

the turbulence in the solar wind plasma as

$$C \cdot q^{-3} \cdot r^{-\beta} \quad \dots(6.b)$$

(where C is a constant, r is the Heliocentric distance and $\beta = 4$, (Armstrong and Coles, 1978)), computations of Marians (1975) were scaled to the present conditions. Curves of scintillation index, m vs solar elongation, e for various source sizes at 103 MHz are plotted (Fig. 6.6). The power-law curve for 0.2 arcsec. source size is a best-fit to these IPS data (Fig. 6.7). Comparison of Figs. 6.5 and 6.6 shows that the power-law model is a better fit to the 3C 144 IPS data of 103 MHz.

To estimate the angular size of 3C 144, theoretical curves of scintillation index vs. solar elongation for various source sizes and for a gaussian irregularity spectrum have been used (Readhead, Kemp and Hewish, 1978) (Fig. 6.8). From these curves another theoretical curve of $m(28^\circ)/m(70^\circ)$ for various source sizes has been plotted (Fig. 6.9).

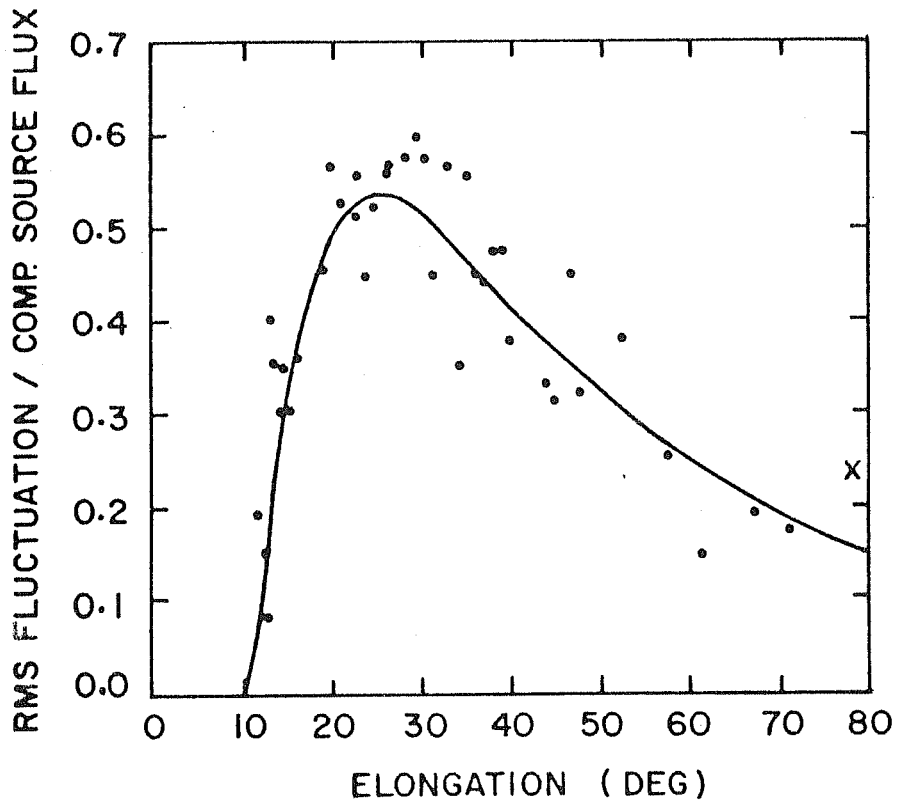


Fig. 6.7 R.M.S. fluctuation of the compact source flux at 103 MHz normalized by the compact source flux is plotted against solar elongation. The continuous curve is for power law model for 0.2 arcsec source. The model computations were made using the method of Marians (1975).

Now from our observational curve (m vs. ϵ) of Fig. 6.2, $m(28^\circ)/m(70^\circ)$ was calculated to be about 3. Using Fig. 6.9 the angular size of the scintillating source was estimated to be about 0.16 arcsec.

6.4 Discussion and Conclusion

There is a discrepancy in the flux values of the compact source in the Crab Nebula obtained from the IPS observations and those obtained from the extrapolation of the VLBI and lunar occultation observations of the pulsed emission. This suggests that either the pulsed radiation is getting smeared due to multipath scattering in the interstellar medium, resulting at low frequencies into a source of continuum radiation, or else, there is another compact source near the pulsar.

In the latter case, the scintillations would add incoherently. The IPS observations at 103 MHz would then imply that the square-root of the sum of the squares of their fluxes must equal 100 Jy. This means that the compact continuum source would have to be stronger than the pulsar i.e. $[S_1^2 + S_2^2]^{1/2} \approx 100$ Jy. The value of S_1 , the pulsar flux extrapolated from the spectrum, is about 45 Jy. Therefore, S_2 , the compact continuum flux = 89 Jy which is larger than the pulsar flux. But high frequency VLBI observations do not indicate a double source (Vandenberg et al. 1973). For frequencies ≤ 300 MHz, the pulsar (0531+21) pulse appears as a sharp rise followed by an

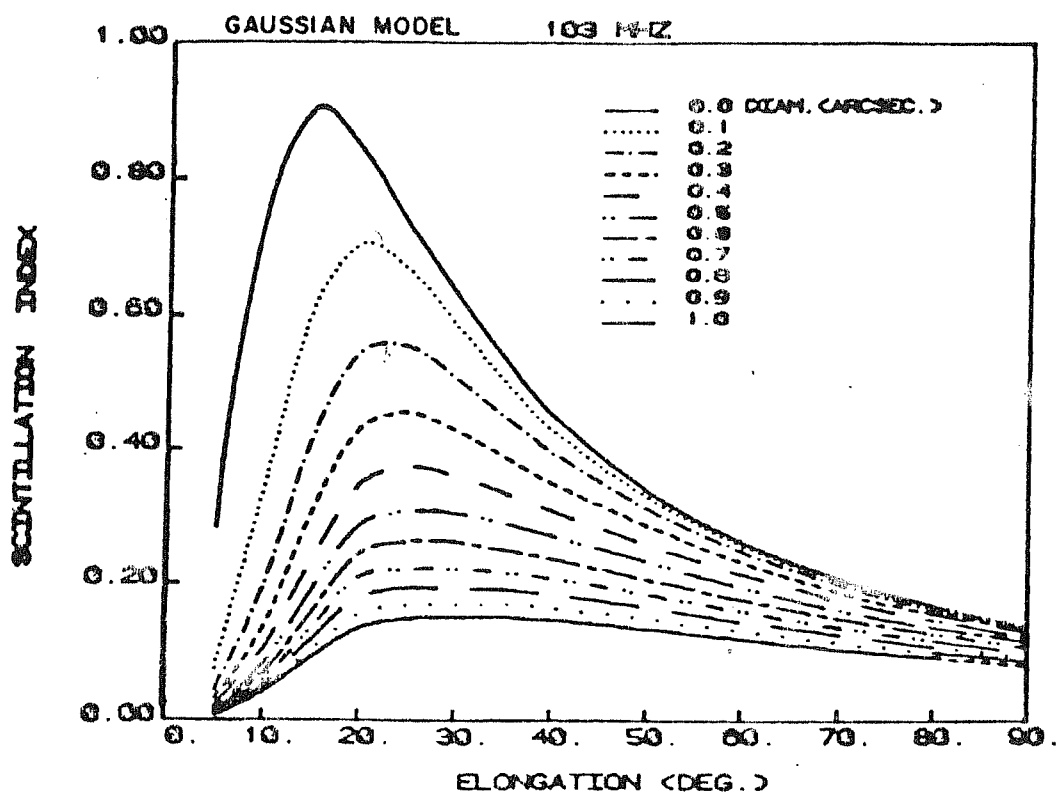


Fig. 6.8 103 MHz theoretical curves of scintillation index vs. solar elongation for various source sizes for a gaussian model. After Readhead et al. 1978.

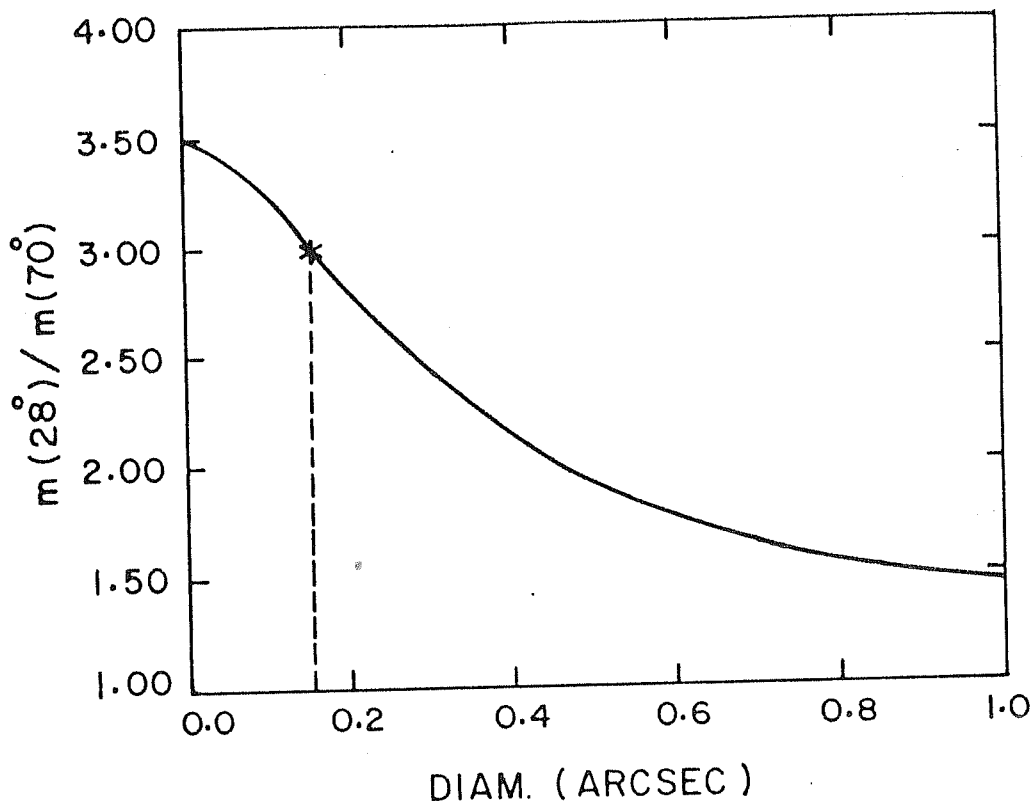


Fig. 6.9 Theoretical curve of ratios of scintillation indices $[m(28^\circ)/m(70^\circ)]$ vs. source size, using fig. 6.8.

exponential decay. As the time constant of the exponential decay is about 13 ms at 115 MHz with the pulsar period of 33 ms, the pulse is smoothed out due to interstellar scattering (ISS). This results into a continuous signal. Assuming a uniform irregularity structure of the interstellar medium between the pulsar and the observer (scattering screen half-way in between), the apparent angular diameter of the pulsar has been estimated using intensity scintillation analysis (Ratcliffe, 1956; Salpeter, 1967). At 115 MHz, the angular size of the compact source was estimated to be about 0.12 arcsec. (Sutton, 1969). Using $\theta_d \propto \lambda^2$, (Cronyn, 1970) where λ is the operating wavelength, this size θ_d at 103 MHz turns out to be about 0.134 arcsec. This is the expected value of the angular size of the compact source, whereas observationally at 103 MHz it is calculated to be about 0.16 ± 0.02 arcsec. Thus our observations at 103 MHz indicate that there is a 23% rise in the angular diameter of the compact source compared to its expected value.

CHAPTER SEVEN

FUTURE WORK

In this chapter some possibilities of future work are discussed. These are of two kinds:

- I. A problem emerging from the work presented in this thesis deals with enhanced scintillation of a radio source occulted by the ion-tail of a comet.
- II. A problem dealing with the sky survey of scintillating radio sources at 103 MHz using enlarged Thaltej telescope.

In what follows, a brief description of these problems is presented.

I. Enhanced scintillation of a radio source by ion-tail
of a comet

In chapter 4, four observations made at different times and at various frequencies are reported. Two of these observations report that the ion-tails of comets produce scintillations of compact radio sources, while the other two report no enhancement of scintillations attributable to the cometary ion-tails. Thus, there seems to be an ambiguity of whether or not cometary plasma tails are capable of producing enhanced scintillations of compact radio sources. For successful observations of strong scintillations produced by cometary tails, following three conditions must be fulfilled:

- (i) The radio source to be observed should be sufficiently away from the Sun to minimize the background scintillation (IPS) produced by solar plasma irregularities. Such a geometry was possible in the case of Alurkar et al. (1986) and Slee et al. (1987).
- (ii) The comets should have strong ion-tails. Generally, ion-tails of about 10° are developed when bright comets are within 1-2 AU of the Sun.
- (iii) It would be preferable to make such observations simultaneously at more than one widely spaced sites. These frequencies should be ≤ 300 MHz as scintillations are inversely proportional to the operating

frequency as a result of the characteristics of the IPM.

The most important and interesting problem would be to make observations using 3-site IPS observatory during the occultation of a radio source by the cometary ion-tail, to measure the velocity of the plasma in the tail. There have been a few attempts to measure this velocity using different techniques such as Fabry-Perot interferometer (Hoppler et al. 1975). This technique gave a velocity in the range of 20-40 Km/s. With the precise knowledge of this velocity one can determine the scale-sizes of the irregularities, instead of assuming them. Further calculation would provide plasma density in the ion-tail and its r.m.s. deviation.

II. Sky survey of scintillating radio sources at 103 MHz

Currently, expansion of the radio telescope at Thaltej is going on under the project "Indo-US Cooperative Project on IPS". The area of the antenna will be doubled to about 20,000 m². 32 dual-channel total-power receivers are to be used under this scheme. This versatile system will be able to scan the overhead sky in 24 hrs. in 32 closely-spaced strips each of about 2° wide in declination. Consequently, about 1,500 scintillating sources of flux densities ≥ 1 Jy are expected to be detected by this system. This improved system will be able to cover the sky between 53°N and 30°S in declination (if grating lobes are also used).

It is proposed that a sky survey of scintillating radio sources should be carried out. This will help in studying the structure of compact sources - whether they are single or double layer sources. A comparison of angular sizes of these sources should be made with those at different frequencies. This can give an idea of whether the angular sizes of the sources and their structures vary with frequency. Additionally, one can use this information obtained from the above survey for mapping of the plasma turbulence in the IPM. Such maps, called 'g-maps' (Hewish et al. 1985), have been shown to be useful in detecting travelling interplanetary disturbances such as shocks or transients originating from the Sun. Statistically a good sample of these events would help in understanding the origin of solar disturbances. At present there is a difference of opinion regarding whether these disturbances originate in solar flares or in coronal holes.

This survey should be compared with that of the Cambridge made at 81.5 MHz. This will help resolve some of the confusion about scintillating sources detected by Cambridge astronomers.

REFERENCES

1. Alfven, H., 1957, *Tellus*, **9**, 92.
2. Alurkar, S.K., H.O. Vats, R.V. Bhonsle & A.K. Sharma, 1985, *Proc. Indian Acad. Sci. (Earth Planet. Sci.)*, **94**, 77.
3. Alurkar, S.K., R.V. Bhonsle & A.K. Sharma, 1986, *Nature*, **322**, 439.
4. Ananthakrishnan, S., S.M. Bhandari & Pramesh Rao, 1975, *Astro. Sp. Sci.*, **37**, 275.
5. Ananthakrishnan, S., P.K. Manoharan & V.R. Venugopal, 1987, *Nature*, **329**, 698.
6. Andrew, B.H., N.J.B.A. Branson, & D. Wills, 1964, *Nature*, **203**, 171.
7. Antonova, T.D., V.G. Panadzhyan & A. Pynzar, 1971, *Soviet Astr.-AJ*, **15**, 13.
8. Armstrong, J.W. & W.A. Coles, 1972, *J.G.R.*, **77**, 4602.
9. Armstrong, J.W., W.A. Coles, J.J. Kaufman & B.J. Rickett, 1973, *Ap. J.*, **186**, L135.
10. Armstrong, J.W. 1975, Ph.D. Thesis, University of California, San Diego.
11. Armstrong, J.W. & W.A. Coles, 1978, *Ap.J.*, **220**, 346.
12. Behr, A. & H. Siedontopf, 1953, *Z. Astrophys.*, **32**, 19.
13. Bell, S.J. & A. Hewish, 1967, *Nature*, **213**, 1214.

14. Biermann, L., 1951, *Zs.f. Astrophys.*, **29**, 274.
15. Booker, H.G., 1981, *J. Atmos. Terr. Phys.*, **43**, 1215.
16. Bougeret, J.L., 1981, *Astron. Astrophys.*, **96**, 259.
17. Brandt, J.C., 1970, "Introduction to The Solar Wind", W.H. Freeman & Company, San Francisco.
18. Butler, J.I., 1966, "Microwave Scanning Antennas, III", ed. R.C. Hansen, N.Y. Acad. Press, 254.
19. Chapman, S., 1957, *Smithsonian Contrib. Astrophysics*, **2**, 1.
20. Chandra, H., A.V. Janve, G. Sethia & R.G. Rastogi, 1979, *Indian J. Radio Space Phys.*, **8**, 1.
21. Chernov, Lev A., 1960, "Wave Propagation in a Random Medium", McGraw-Hill, New York.
22. Cohen, M.H., E.J. Gundermann, & D.E. Harris, 1967, *Ap. J.*, **150**, 767.
23. Cohen, M.H., E.J. Gundermann, H.E. Hardbeck & L.E. Sharp, 1967, *Ap. J.* **147**, 440.
24. Cohen, M.H., 1969, *Ann. Rev. Astr. Astrophys.*, **7**, 619.
25. Coles, W.A. & S. Maagoe, 1972, *J.G.R.* **77**, 5622.
26. Coles, W.A., B.J. Rickett & V.H. Rumsey, 1974, "The Solar Wind III", p.351, (ed. C.T. Russel), Univ. of California, Los Angeles, NASA Scientific & Technical Information Office, Washington D.C.
27. Coles, W.A. & B.J. Rickett, 1976, *J.G.R.*, **81**, 4797.
28. Cole, T.W. & O.B. Slee, 1980, *Nature*, **285**, 93.

29. Conway, R.G., W.L.H. Shuter & P.A.T. Wild, 1961, Observatory, 81, 106.
30. Cronyn, W.M., 1970, Ap. J., 161, 755.
31. Delaney, W.P., 1962, IRE Trans. Mil. Elec., MIL-6, 179.
32. Dennison, P.A. & M. Wiseman, 1968, Proc. A.S.A., 1, 142.
33. Duffett-Smith, P.J., 1976, Ph.D. Thesis, University of Cambridge.
34. Dryer, M., 1987, "Wind and Earth", (20-35) ed. by S.I. Akasofu and Y. Kamide by Terra Scientific Publishing Co. (TERRA PUB), Tokyo.
35. Erickson, W.C., T.B.H. Kuiper, T.A. Clark, S.H. Knowles & J.J. Broderick, 1972, Ap. J., 177, 101.
36. Ershkovich, A.I., 1980, Space Sci. Rev., 25, 3.
37. Gapper, G.R. & A. Hewish, 1981, MNRAS, 197, 209.
38. Gapper, G.R., A. Hewish, A. Purvis & P.J. Duffett-Smith, 1982, Nature, 296, 633.
39. Georges, T.M. 1968, J. Atmos. Terr. Phys., 30, 735.
40. Hajivassiliou, C.A. & P.J. Duffett-Smith, 1987, MNRAS, 229, 489.
41. Hewish, A. & S.E. Okoye, 1964, Nature 203, 171.

42. Hewish, A., P.F. Scott & D. Wills, 1964, *Nature*, Lond. 203, 1214.
43. Hewish, A. & S.E. Okoye, 1965, *Nature*, 207, 59.
44. Hewish, A. & M.D. Symonds, 1969, *Planet. Space Sci.*, 17, 313.
45. Hewish, A. 1972, "Solar Wind", p. 477, (eds. Sonett, C.P. et. al.), Asilomar Conference Grounds, Pacific Grove, California, NASA Scientific & Technical Information Office, Washington D.C.
46. Hewish, A. 1980, *Nature*, 285, 95.
47. Hewish, A., S.J. Tappin & G.R. Gapper, 1985, *Nature*, 314, 137.
48. Hewish, A. & P.J. Duffett-Smith, 1987, *Planet. Space Sci.*, 35, 487.
49. Hoppler, D., S.R.J. Reynold, F.L. Roesler, F. Scherb & J. Trauger, 1975, *Ap. J.*, 202, 276.
50. Houminer, Z., 1971, *Nature*, 231, 165.
51. Ip, W.H. & W.I. Axford, 1982, "Comets", p.588, ed. L.L. Wilkening, Univ. Arizona, Press Tucson.
52. Ishimaru, A., 1972, *IEEE, Trans. Ant. Prep.*, 20, 10.
53. International Halley Watch (IHW) Newsletter No.7, June 18, 1985, Ed. Stephen J. Edberg.
54. Jain R.K., 1977, *Indian J. Radio Space Phys.*, 30, 163.
55. Jockers, K. & R. Lust, 1973, *Ap. J.*, 26, 113.

56. Jokipii, J.R., 1973, Ann. Rev. Astr. and Ap., 11, 1.
57. Kakinuma, T. & M. Kojima, 1984, "Solar Wind Speed from IPS Measurements", The Research Institute of Atmospherics, Nagoya University, Toyokawa, Japan.
58. Kemp, M.C., 1976, Ph.D. Thesis, Cambridge Univ. UK.
59. Kraus, J.D. 1966, "Radio Astronomy". McGraw-Hill, New York.
60. Kenneth R. Lang, 1971, "The Crab Nebula", 91-96 (IAU) eds. Davies & Smith.
61. Lee, L.C. & J.R. Jokipii, 1975a, Ap. J., 196, 695.
62. Lee, L.C. & J.R. Jokipii, 1975b, Ap. J., 206, 439.
63. Lee, L.C., 1976, Astrophys., 210, 254.
64. Little, L.T. & A. Hewish, 1966, MNRAS, 134, 221.
65. Little, L.T., 1976, "Methods of Experimental Physics, 12C, p.118, ed. M.L. Meeks, Ch. 4.7 (Academic Press, New York).
66. Lotova, N.A. 1975, Soviet Phys. Uspekhi, 18, 292.
67. Lovelace, R.V.E., E.E. Salpeter & L.E. Sharp, 1970, Ap. J., 159, 1047.
68. Mariani, M., 1975, Radio Science, 10, 115.
69. Matveenko, L.I. & A.V. Pynzar, 1969, Soviet Astr.-AJ, 13, 433.
70. Mercier, R.P., 1962, Proc. Camb. Phil. Soc., 58, 382.

71. Okoye, S.E. & A. Hewish, 1967, MNRAS 137, 287.
72. Okoye, S.E. & A. Hewish, 1968, J. Atmos. Terr. Phys., 30, 163.
73. Parker, E.N. 1958, Ap. J., 128, 664.
74. Parker, E.N. 1963, "Interplanetary Dynamical Processes", John Wiley & Sons, New York.
75. Rankin, J.M., J.M. Comella, H.D. Craft, D.W. Richards, D.B. Campbell & C.C. Counselman, 1970, Ap. J. 162, 707.
76. Ratcliffe, J.A., 1956, Rep. Progs. Phys., 19, 188.
77. Readhead, A.C.S., 1971, MNRAS, 155, 185.
78. Readhead, A.C.S. & A. Hewish, 1974, Mem. R.A.S., 78, 1.
79. Readhead, A.C.S., M.C. Kemp & A. Hewish, 1978, MNRAS, 185, 207.
80. Rees, R.G., P.J. Duffett-Smith, S.J. Tappin, & A. Hewish, University of Cambridge, Dept. of Physics, Pre-print No. 1178.
81. Rickett, B.J., 1970, MNRAS, 150, 67.
82. Rickett, B.J., 1973, J.G.R., 78, 1543.
83. Rumsey, V.H., 1975, Radio Sci., 10, 107.
84. Salpeter, E.E., 1967, Ap. J. 147, 433.

85. Sardesai, D.V., R.K. Rai, G.D. Vyas & H. Chandra, 1983, Indian J. Radio Space Phys., 12, 18.
86. Scott, S.L., 1978, Ph.D. Thesis, Univ. of California, San Diego.
87. Shishov, V.I., 1975, Astron. Zh., 52, 369.
88. Sime, D.G. 1976, Ph.D. Thesis, Univ. of California, San Diego.
89. Slee, O.B., D. McConnell, J. Lim & A.D. Bobra, 1987, Nature, 325, 699.
90. Sutton, J.M., 1969, Paper presented at the 131st Meeting of the American Astronomical Society, New York, 8-11 Dec. 1969.
91. Tatarski, V., 1961, "Wave Propagation in a Turbulent Medium", McGraw Hill, New York.
92. Titheridge, J.E., 1972, Planet. Space Sci., 19, 1593.
93. Vandenberg, N.R., T.A. Clark, W.C. Erickson, G.M. Resch, J.J. Broderick, R.R. Payne, S.H. Knowles, & A.B. Youmans, 1973, Ap. J., 180, L27.
94. Vats, H.O. & M.R. Deshpande, 1980, Proc. Indian Acad. Sci. (Earth Planet. Sci.), 89, 137.
95. Vats, H.O., H.G. Booker & G.J. MajdiAhi, 1981, J. Atmos. Terr. Phys., 43, 1235.
96. Watanabe, T. & T. Kakinuma, 1972, Publ. Astr. Soc., Japan, 24, 459.
97. Watanabe, T., T. Kakinuma, M. Kojima & K. Shibasaki, 1973, J.G.R., 78, 8364.

98. Whipple, F.L., 1950, Ap. J., 111, 375.
99. Whipple, F.L., 1950, Ap. J., 111, 464.
100. Whipple, F.L., 1955, Ap. J. 121, 750.
101. Whitfield, G.R. & J. Hoggom, 1957, Nature 180, 602.
102. Wurm, K., 1968, Icarus, 8, 287.
103. Yeh, K.C. & C.H. Liu, 1974, Rev. Geophys. Space Phys., 12, 193.